The Gravity Field over the Bane Dome in Giles County, Virginia

by

Michael J. Moses

Thesis submitted to the Faculty of the

Virginia Polytechnic Institute and State University

in partial fulfillment of the requirements for the degree of

Master of Science

in

Geophysics

APPROVED:

E. S. Robinson, Chairman

John K. Costain

Lynn Glover, III

June 30, 1988

Blacksburg, Virginia

The Gravity Field over the Bane Dome in Giles County, Virginia

by

Michael J. Moses

E. S. Robinson, Chairman

Geophysics

(ABSTRACT)

The Bouguer gravity field, determined from 395 measurements in Giles County, Virginia exhibits a broad positive anomaly approximately 12 mgal in amplitude situated over the Bane Dome, and several smaller anomalies of a few milligals amplitude. For the most part they are produced by the distribution of relatively high density carbonate rocks and lower density clastic rocks within the dome.

These anomalies can be explained by two contrasting interpretations of the structure of the Bane Dome. One interpretation, represented by the geologic cross sections of Woodward and Gray (Woodward, 1985) and Bartholomew (personal communications, 1987) suggests that the dome is cored by a relative abundance of high density carbonate rocks transported by overthrusting within the Narrows thrust sheet. Because the gravity anomalies can be entirely explained by sources confined to the Narrows thrust sheet, this interpolation precludes the existence of significant lateral density contrasts associated with deeper structure beneath the decollement zone in the Rome Formation.

The contrasting interpretation represented by the cross section of Gresko (1985), suggests a smaller proportion of carbonate rocks in the core of the dome due to duplex structures in the lower density clastic rocks. This interpretation proposes high angle faults with associated lateral density contrasts in the deeper rocks underlying the decollement. Because sources within the Narrows thrust sheet are insufficient to completely account for the gravity anomalies, the density contrasts associated with deeper structure are required.

The Bouguer gravity field can be separated into regional and residual parts. The regional field is caused by changes in crustal thickness known independently from the seismic measurements of

James, Smith, and Steinhart (1968). The remaining residual field can be explained in terms of anomaly sources within the upper 10 km of the crust.

Acknowledgements

I would like to thank for suggesting the study, editing the manuscript, and his guidance and encouragement through the long years it took to complete this study. reviewed the manuscript and made many helpful suggestions. established gravity stations in the area. kindly made available the arrays of elevation data used for terrain corrections.

I am especially indebted to my daughter, , for her love and understanding during this project. This study would not have been possible without the aid of my father, who taught me to deal with adversity.

This research was partially supported by a graduate fellowship from Chevron, Inc.

Table of Contents

List of Illustrations

Introduction

The Bane Dome is located in Giles Co., Va. (Figure 1) in the Valley and Ridge Province of the southern Appalachian Mountains as well as within the Giles Co. seismic zone. It is a doubly plunging anticline situated in a folded and thrust faulted terrain. This clearly defined structure invites speculation. For more than three decades the Bane Dome has been a focal point in discussions about the relative importance of low angle thrust faulting within the Paleozoic sedimentary sequence compared with high angle basement faulting in the tectonic development of the southern Appalachians (Rodgers, 1949, Cooper, 1964). Interpretations of recently acquired seismic reflection data (Edsall, 1974, Gresko, 1985) argue that the structures in the area are related mainly to thrust faulting with little or no involvement of basement rocks. This thin-skinned tectonic interpretation asserts that the thrust faulting originates along a major decollement in the relatively incompetent Cambrian-age Rome shale.

The location of the Bane Dome within the Giles Co. seismic zone makes the question of deep basement tectonics important in this study. Seismicity within Giles Co. is believed to occur on reactivated normal faults which were the result of rifting during late Precambrian Iaeptan time (Bollinger et al, 1985). They suggest that these faults lie within the basement beneath the Valley and Ridge, and due to reactivation under the current compressive stress regime, now appear to be undergoing strike-slip displacement within the Giles Co. seismic zone.

Reflection seismic surveys in this area (Figure 1), while clarifying the importance of thin-skinned tectonics, have not resolved questions concerning the subsurface distribution of rock units within the dome; nor have these surveys clarified the nature and extent of basement faulting. Because of karst terrain and the abundance of high velocity carbonate rocks, conventional P-wave seismic reflection surveys give somewhat unclear results. Although shear wave seismic reflections (Gresko, 1985) appear to give better resolution, the survey lines are restricted to three unpaved secondary roads on the northwest flank of the Bane Dome which do not cross the axis of the structure.

In an effort to contribute to the resolution of these questions, a gravity survey was undertaken. A total of 395 gravity stations were established in four 7.5 minute quadrangles, Narrows, Pearisburg, White Gate, and Staffordsville, surrounding the Bane dome. Interpretation of Bouguer gravity variations involves comparisons with gravity profiles calculated for different two-dimensional models of density distribution to obtain an improved picture of the Bane Dome and further information on the extent of basement faulting beneath the dome. These two-dimensional models are based upon three geologic cross-sections that display different interpretations of the structure of the dome. The discussion of gravity anomalies also addresses questions concerning separation of regional and local anomalies, and the density values used in gravity reduction.

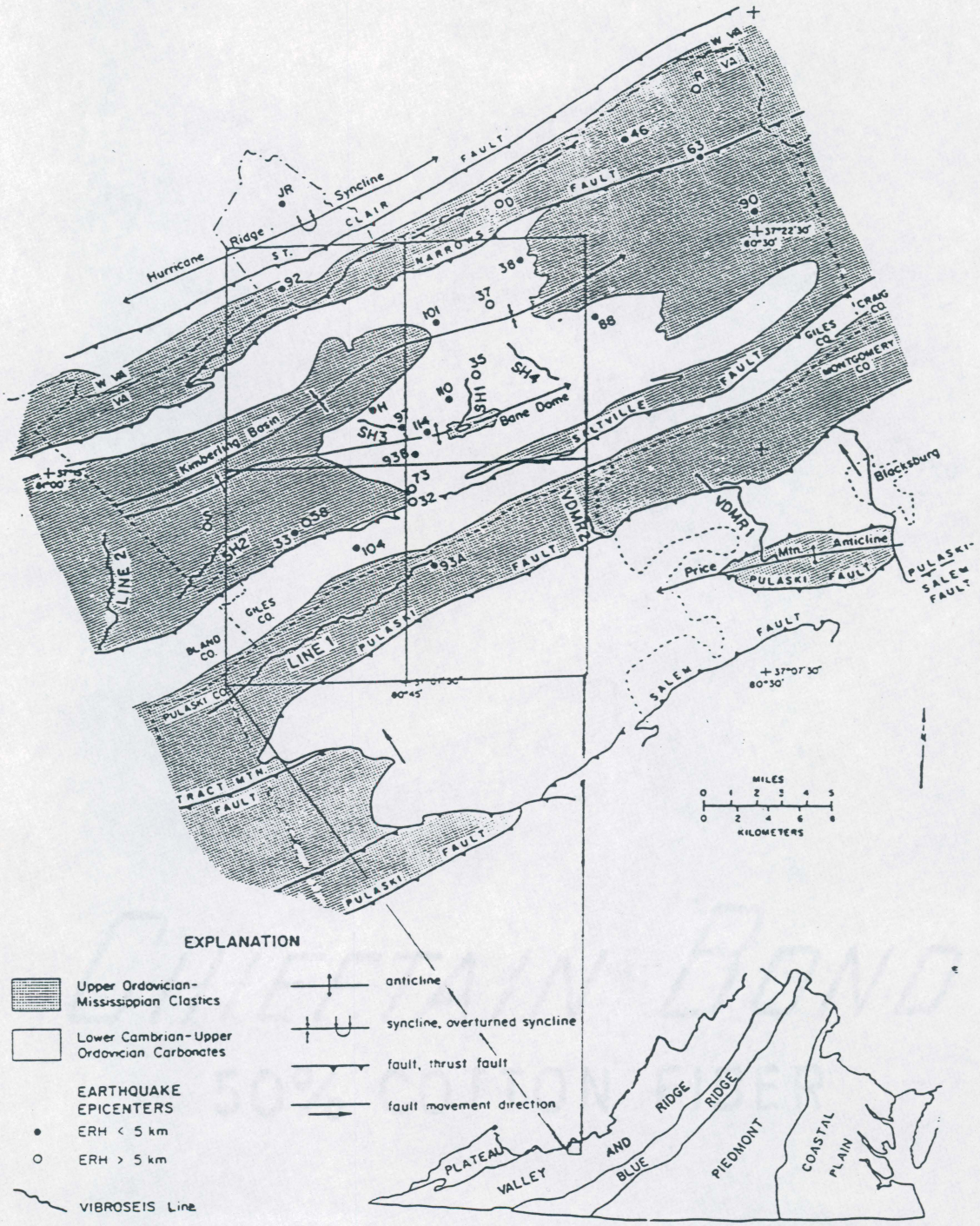

Figure 1. Location Map: Map of study area with location of seismic lines and earthquake epicenters (Modified from Gresko, 1985).

Geology

The Valley and Ridge Province of the southern Appalachians is characterized by folded and thrust faulted sedimentary rocks. The region is dominated by broad synclines which form the topographic highs within the study area. The structures and thrust faults within the area trend N60-65E (Figure 2), which is the dominant trend in the southern Appalachians. The Bane Dome is a doubly plunging anticline located within the Narrows thrust sheet. It is bordered to the north by the Pearisburg syncline and to the south by the Dublin syncline. Along strike to the southwest is the Kimberling basin and to the northeast is the Johns Creek syncline.

Stratigraphy

Knowledge of the stratigraphic units in the region of a gravity survey is of central importance in the interpretation of gravity anomalies. Variations of Bouguer gravity are related to the contrasting densities of the rock units present, and to the relative abundance of these units. Among the many sources of information about the stratigraphy in this part of the Valley and Ridge Province are Butts (1942) and Cooper (1961). For purposes of this study, rock density information determined by Edsall (1974) and Kolich (1974) was used. These rock density values (Table 1) were

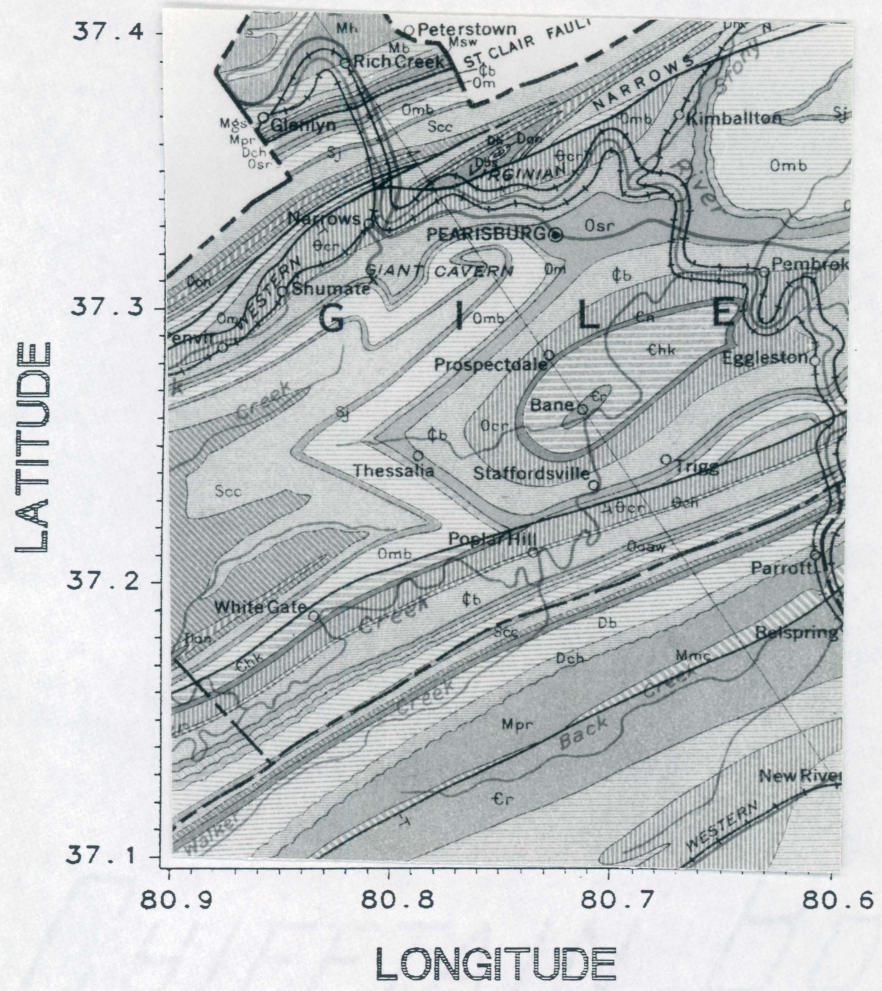

Mississippian	Mh	Hinton formation
	Mb	Bluefield shale
	Mgs	Gasper limestone
	Msw	St. Louis limestone
	Mmc	Maccrady shale
	Mpr	Price formation
Devonian	Dch	Chemung formation
	Db	Brallier formation
	Dbs	Romney shale
	Dh	Helderberg limestone
Silurian	Scc	Clinton formation
	Sj	Juniata formation
Ordovician	Omb	Martinsburg shale
	Om	Moccasin limestone
	Ocaw	Blount group
	Osr	Stone River group
	Och	Cheputepec limestone
	Ocr	Copper Ridge dolomite
Cambrian	Cb	Beekmantown dolomite
	Cn	Nolichucky shale
	Chk	Honaker dolomite
	Ce	Elbrook dolomite
	Cr	Rome formation

Figure 2. Geologic Map: Geologic map of the Bane Dome area from Butts (1933).

determined from laboratory measurements on representative wet and dry samples of rock units exposed in the area.

The stratigraphic units exposed in the study area are mostly Paleozoic sedimentary rocks. Oldest in the stratigraphic sequence is a sedimentary package dating from early Cambrian time, which consists of the Unicoi Sandstone, the Hampton Shale, the Erwin Sandstone, and the Shady Dolomite. Based upon density information in Edsall (1974) the average density of this package is approximately 2.73 gm/cc (Gresko, 1985).

Next in the stratigraphic sequence is the lower to middle Cambrian Rome Formation which consists of mudstone with some minor interbedded dolomite (Butts, 1933). It contains several good index fossils including trilobites of genus Olenellus which are restricted to the lower Cambrian as well as trilobites of the genera *Alokistocarella* , *Anoria* , *Elrathiella* , *Glossopleura* , and *Solenopleurella* , all of which are restricted to the middle Cambrian (Butts, 1933). Within the relatively incompetent Rome Formation is the decollement zone where most of the thrust faults in the southern Appalachians appear to originate (Perry et al, 1979). Everywhere this formation is fault bounded at the base (Gresko, 1985). The dolomite beds have a density close to 2.83 gm/cc, while the much more abundant shale facies have an average density of 2.67 gm/cc (Table 1).

Overlying the Rome Shale is the middle Cambrian Honaker Dolomite. This formation consists of massive bedded dolomites and contains few fossils. This formation has the highest density within the study area, which is close to 2.85 gm/cc (Table 1)

The upper Cambrian-lower Ordovician Knox Group is also primarily a massively bedded dolomite. Unlike the underlying Honaker, however, this pale to dark gray dolomite contains a few biostratigraphically useful conodonts which were used in reevaluating (Perry et al, 1979) the earlier interpretation (Cooper, 1964) that the Rome Shale at the core of the Bane Dome overlays the lower Cambrian Shady Dolomite. The interpretation of Cooper suggested basement involvement in the thrust faulting, however discovery of conodonts in cores from a well drilled on the crest of the dome showed that the Rome shale was underlain by the Knox group (Perry et al, 1979). This latter interpretation is consistent with the thin-skinned thrusting and folding model unrelated to local basement tectonics. The Knox group is poorly exposed within a window at the crest of the dome

(Perry et al, 1979). It is made up of the following units: The Cambrian Copper Ridge Dolomite; Cambrian Copper Ridge Sandstone; Ordovician Chepultepec Dolomite; Ordovician Chepultepec Limestone; Ordovician Longview Limestone; Ordovician Kingsport Dolomite; and the Ordovician Upper Knox Dolomite. Density values for these units are given in Table 1. The Knox group has an average density of approximately 2.80 gm/cc (Kolich, 1974).

The Ordovician Martinsburg Formation is the last significant formation located in the Bane Dome area. Outcrops of the Martinsburg Formation within the study area are rare, but where it is seen it is a folded mass of light and medium bluish-gray limestone with interbedded gray and tan shale (Whitman, 1960). In general the Martinsburg formation consists of 300-400 meters of interlayered limestone, siltstone, sandstone, and calcareous mudstone beds with limestone more abundant in the lower half and shale dominating the upper portion (Mullenax, 1981). The average density of the Martinsburg shale is 2.70 gm/cc (Kolich, 1974). Younger sedimentary rocks ranging in age from Late Ordovician to Mississippian do not appear to exist in the Bane Dome, although they are exposed in the bordering synclines.

Table 1. Density Values

Density values for sedimentary rocks in the Bane Dome region (Edsall, 1974 and Kolich, 1974).

Age	Formation	Density	Age	Formation	Density
Mississippian	Price sandstone	2.67		Kingsport dolomite	2.79
	post-Cloyd claystone	2.72		Longview limestone	2.71
	Cloyd conglomerate	2.58		Chepultepec limestone	2.72
	Parrott sandstone	2.62		Chepultepec dolomite	2.83
Devonian	Chemung sandstone	2.61	Cambrian	Copper Ridge sandstone	2.71
	Millboro shale	2.74		Copper Ridge dolomite	2.81
Silurian	Keefer sandstone	2.64		Elbrook dolomite	2.80
	Rose Hill sandstone	3.07		Honaker dolomite	2.85
	Tuscarora sandstone	2.64		Rome shale	2.67
Ordovician	Juniata sandstone	2.62		Rome dolomite	2.83
	Martinsburg shale	2.70		Shady dolomite	2.84
	Eggleston conglomerate	2.65		Shady limestone	2.73
	Moccasin shale	2.71		Erwin sandstone	2.59
	Bays sandstone	2.68		Hampton shale	2.71
	Witten limestone	2.68		Unicoi sandstone	2.67
	Liberty Hall shale	2.69	Precambrian	Augen gneiss	2.70
	Lincolnshire limestone	2.70		Amphibolite	3.00
	Five Oaks limestone	2.70		Lynchburg amphibolite	2.97
	New Market limestone	2.72		Lynchburg gneiss	2.64
	Elway limestone	2.68		Grenville gneiss	2.66
	Upper Knox dolomite	2.82			

Structure

The Bane Dome is situated in the Narrows thrust sheet bounded by the Narrows fault on the northwest and by the Saltville fault on the southeast (Figure 3). These faults together with the St. Clair Fault, which is farther to the northwest, and the Pulaski Fault, which is exposed farther to the southeast, all originate along the decollement zone within the middle Cambrian Rome Formation. These thrust faults show varying amounts of displacement. According to Bartholomew (1984) the St. Clair thrust indicates 6 km. of displacement, the Narrows fault 4 km., the Saltville fault 8 km., and the Pulaski fault 80 km. Bartholomew estimated that the St. Clair/Narrows/Saltville thrust sequence shows 15-25% shortening while the Pulaski thrust sheet shows 65-80% shortening.

Several geologic cross sections have been published that present different interpretations of the structure of the Bane Dome. For purposes of this study the three recently compiled cross sections in Figure 4 have been selected for further analysis. Gresko (1985) modified an earlier cross section of Perry and others (1979) to obtain a balanced cross section that incorporates features evident on SH-wave seismic reflection profiles recorded over the northwest flank of the Bane Dome. He showed that the gravity variation over the model was consistent with gravity anomaly patterns presented by Sears and Robinson (1971).

The balanced cross section compiled by N. B. Woodward and D. R. Gray (Woodward, 1985) is also a modification of the earlier cross section of Perry and others, which was constrained by the gravity data of Sears and Robinson (1971) and by information from the F. P. Strader No. 1 test well. This well was drilled to a depth of 440 m at the crest of the Bane Dome by the California Co. in 1948. As pointed out earlier, conodonts from near the bottom of the well indicate that Rome Shale is in thrust contact with the underlying younger Knox Group (Perry and others, 1979).

The third cross section was prepared by M. J. Bartholomew (personal communication, 1987). He modified the earlier cross section of Butts (1933) by extending the rock units to greater depths in a manner consistent with decollement tectonics associated with the incompetent Rome shale.

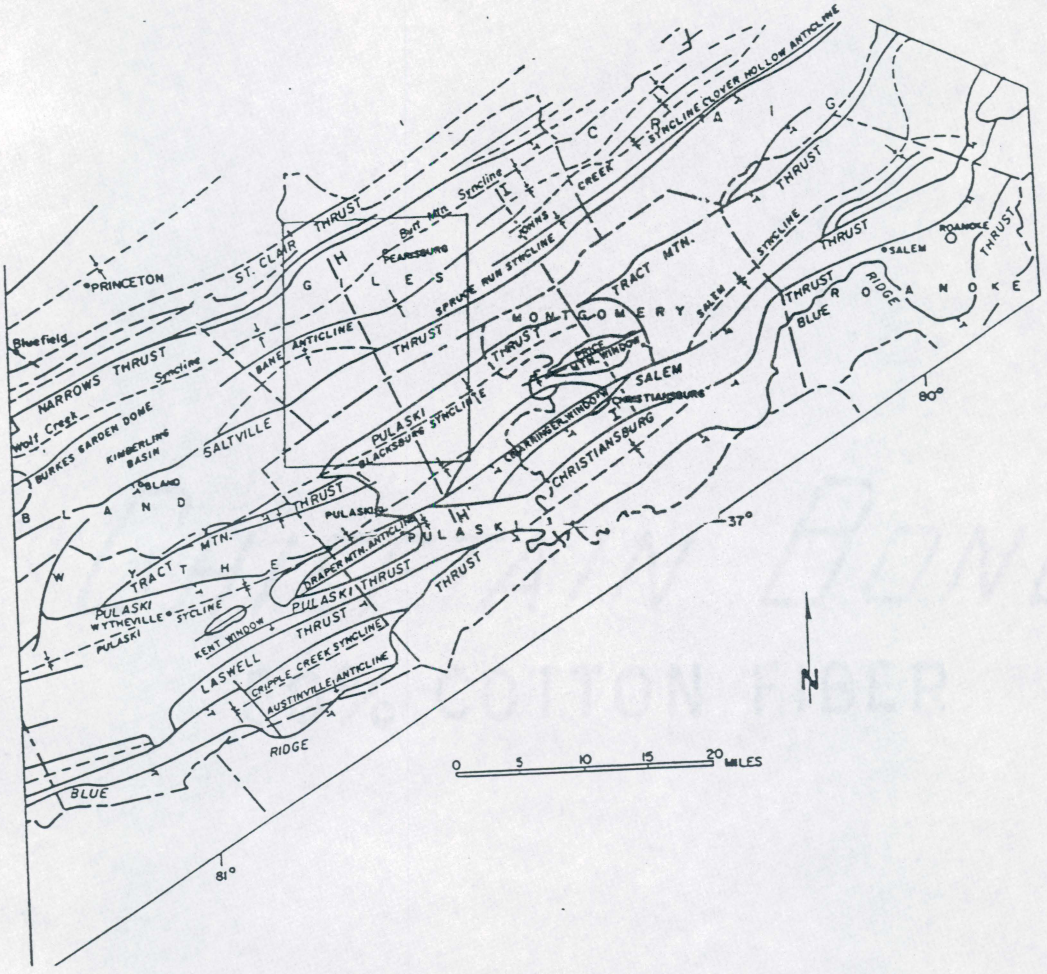

Figure 3. Structure Map: Map showing major structural units in SW Va (Sears and Robinson, 1971).

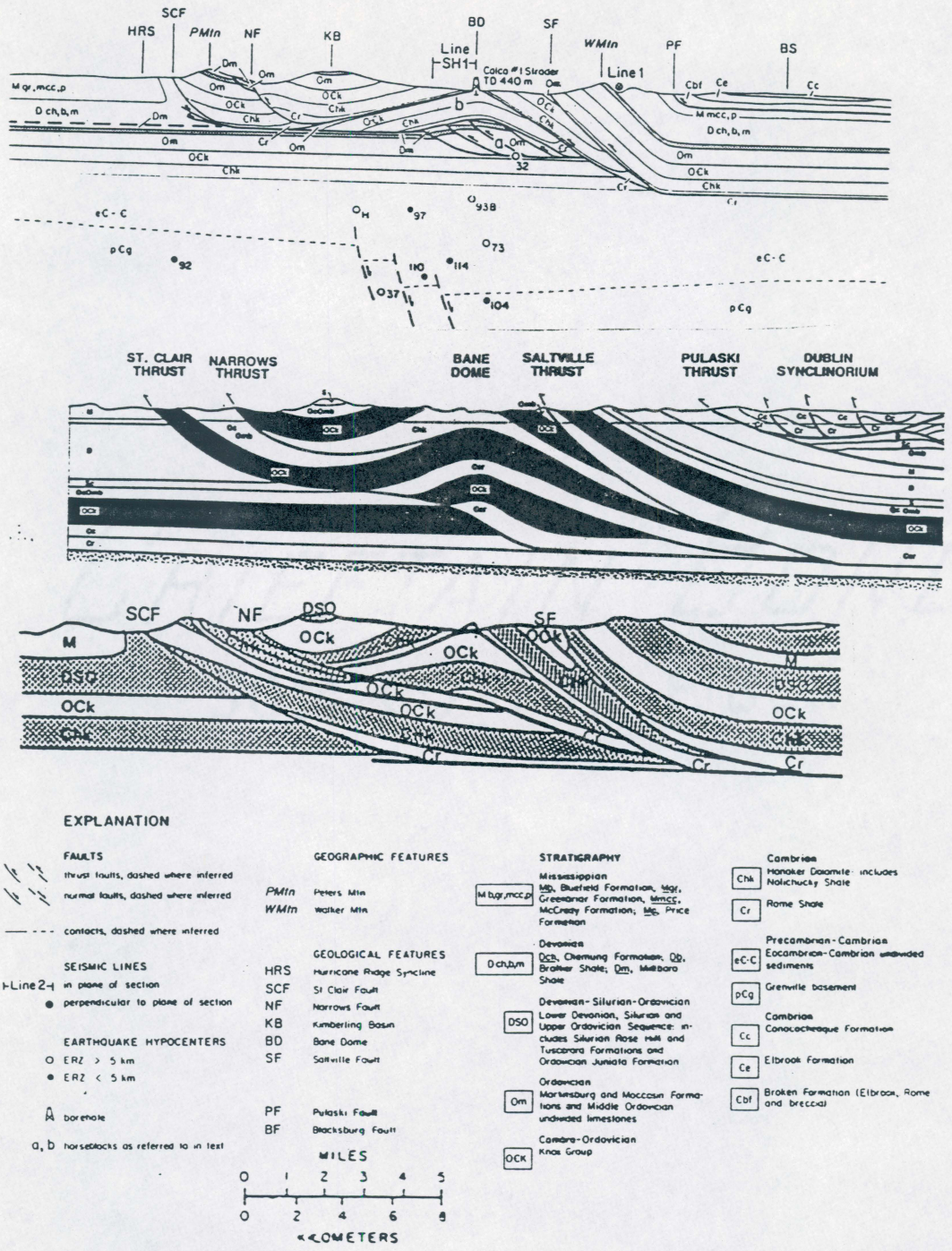

Figure 4. Geologic Models: Geologic cross sections of the Bane Dome from Gresko (1985) (Top), Woodward (1985) (Middle), and Bartholomew (personal communications, 1987) (Bottom).

The three cross sections in Figure 4 are similar to the extent that they represent the Bane Dome as a structure confined to the Narrows thrust sheet. The lower boundary of this thrust sheet is a zone of decollement in the Rome Formation. These cross sections differ from one another in regard to folding and faulting within the Narrows thrust sheet. For example, Gresko (1985) included a section of Martinsburg and Moccasin rocks cut by imbricate thrusts in the core of the dome. This feature, which is based upon interpretation of seismic reflection profiles, does not appear in the other two cross sections. These latter cross sections display a larger total volume of high density carbonate rocks than is shown by Gresko. Furthermore, Gresko includes structural features in the deeper basement rocks that are not seen in the other cross sections. He presents seismic evidence of these high angle faults. The present study examines these differences in terms of the gravity anomalies they would be expected to produce.

Gravity

Gravity measurements were taken at 395 sites between February, 1984 and February, 1986. These sites are indicated in Figure 5. They were located at bench marks, landmarks where elevations are known to within 1 foot, or at locations where elevations can be interpolated to within 5 feet by topographic contours. To distinguish between these sites of varying elevation accuracy, different symbols were used to plot the station positions on the map (Figure 5). All gravity readings were made using Lacoste-Romberg gravimeter No. G-612. Gravity measurements were made at approximately .25 mile intervals along roads across the Pearisburg, Narrows, Staffordsville, and White Gate 7.5 minute quadrangles except where access on the mountains made proper elevation control difficult. These mountain areas, including Walker, Brushy, and Sugar Run mountains, are primarily to the south and west of the Bane Dome.

Gravimeter readings were converted to relative gravity values by using the instrument calibration table provided by the manufacturer. Instrument drift was determined by occupying the Virginia Tech Gravity Base Station at Derring Hall in Blacksburg, Va. before and after each day's survey. The instrument drift was found to be less than .1 mgal on most days and was removed by applying a time dependent linear drift correction to each reading. Corrections for lunar-solar tidal forces were made using the equations of Longman (1959) and a solid earth tidal gravity factor of 1.16 (Robinson, 1974).

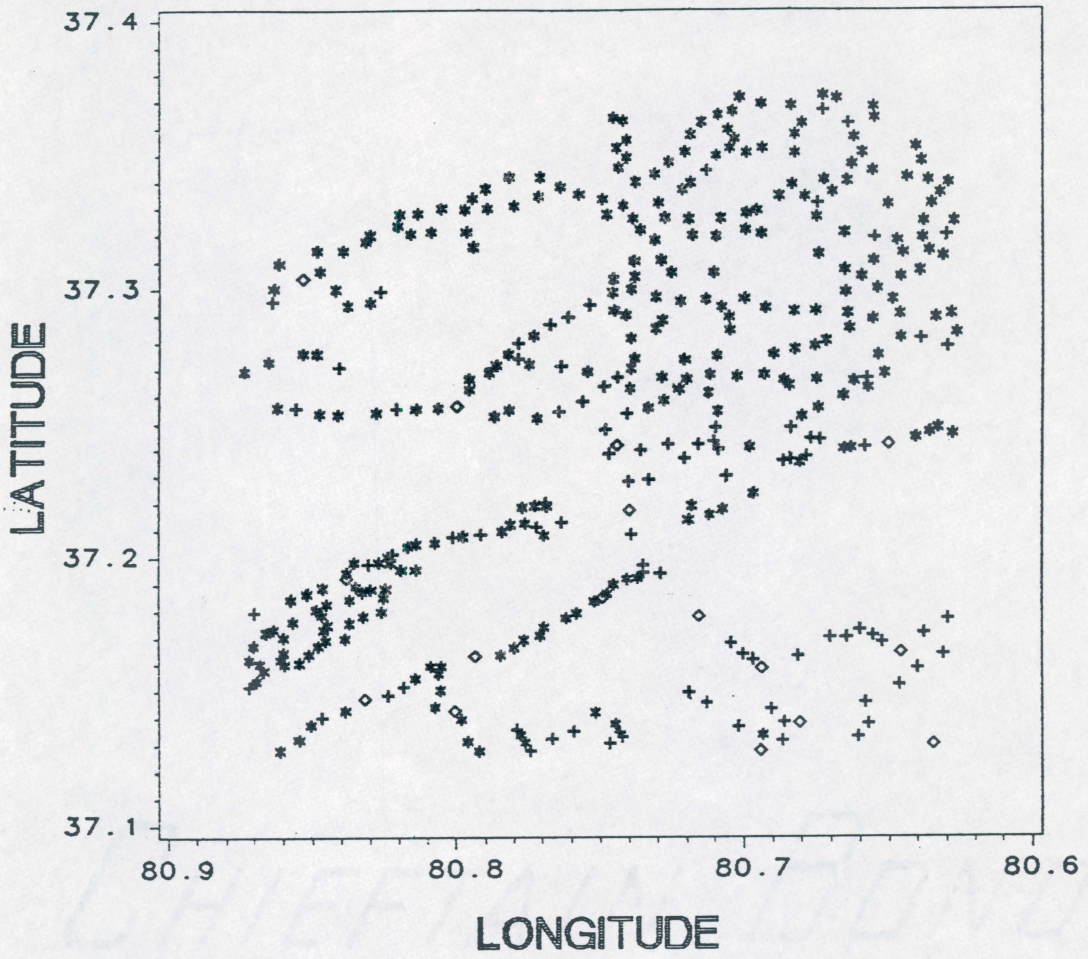

Figure 5. **Station Location Map:** Map of gravity stations where the symbol ◇ represents a benchmark location where elevation is accurate to closer than 1 foot, the symbol + represents a location where elevation accurate to within 1 foot is posted on a 7 ½ minute topographic map, and the symbol * represents a location where elevation is interpolated from topographic contours.

The relative gravity values were converted to observed gravity using the Derring Hall base value of 979718.89 mgals. This value was determined from ties to the National Geodetic Survey absolute gravity base station in Blacksburg, Va. where falling mass measurements were made in July, 1987 and May, 1988.

Gravity data were reduced using the standard formulas for free air gravity Δg_{fa} (Robinson and Coruh, 1988):

$$\Delta g_{fa} = g_{obs} - (g_t - 0.09406h) \tag{1}$$

and complete Bouguer gravity Δg_B (Robinson and Coruh, 1988):

$$\Delta g_B = g_{obs} - (g_t - 0.09406h + 0.01278\rho h - TC) \tag{2}$$

where g_{obs} is observed gravity (mgal), g_t is normal gravity (mgal), h is elevation (ft), ρ is density (gm/cc), and TC is the terrain correction (mgal). The normal gravity was computed using the GRS-67 formula (Woollard, 1979). The elevation, h, in feet was taken from the topographic map and a standard density, ρ = 2.67 gm/cc, was assumed for Bouguer plate corrections and for terrain corrections, TC.

Two procedures were used to calculate terrain corrections necessitated by the rugged relief in the study area. For some stations the well known but time consuming method of Hammer (1939) was used. More suitable for computer calculations is the vertical line approximation method (Stovall and others, in press) which involves representing the terrain by a square grid of elevation values. The mass of terrain within each square grid increment is projected to a vertical line at the center of that increment. A simple formula is then used to calculate the gravitational attraction of each vertical line mass. The results are summed to obtain the terrain correction, TC.

Terrain corrections were calculated using a FORTRAN program and elevations on a 1/3 km by 1/3 km grid covering the study area. These elevations were extracted from a larger data set covering the entire state of Virginia, which was compiled in the School of Forestry and Wildlife Resources at Virginia Tech (Blair Jones, personal communication, 1986). The terrain corrections were computed using the elevations within a 15,000 foot radius of each station. These values were

then checked by computing the Hammer (1939) terrain correction to the J ring for various stations. The results of this comparison gave generally good results (within .05 mgals). For 40 of the stations where the terrain was inadequately sampled by the elevation grid, the vertical line approximation method produced unacceptable terrain correction values. In those cases where the terrain correction exceeded 5 mgals, an alternative value determined by the Hammer graphical method was used. The terrain corrections for the region range from 0 to 4.88 mgals. The lower values are found in the southeastern portion and the higher values in the the central part of the study area. The average terrain correction of 2.3 mgals shows the significance of terrain corrections in this area.

The accuracy of the Bouguer gravity values is largely dependent on the accuracy of the station elevations. As can be seen from equation 2, for a density of 2.67 gm/cc, an elevation uncertainty of 1 foot produces a Bouguer gravity uncertainty of 0.06 mgal. On the basis of this and other sources of error the Bouguer gravity values at stations where elevation is known within one foot are considered accurate to within $\pm$ 0.1. At stations where elevations were interpolated from contours the Bouguer gravity precision is closer to 1/2 mgal.

A Bouguer gravity map of the study area was prepared using the terrain corrected Bouguer gravity values included in Appendix A. These values were contoured using the GCONTOUR routine available from the SAS Institute, Cary, NC. The results in Figure 6 show that Bouguer gravity varies in the range of -62 mgals to -82 mgals. Anomaly patterns indicate alignments trending approximately N60E which is close to the principal structural trend in the area.

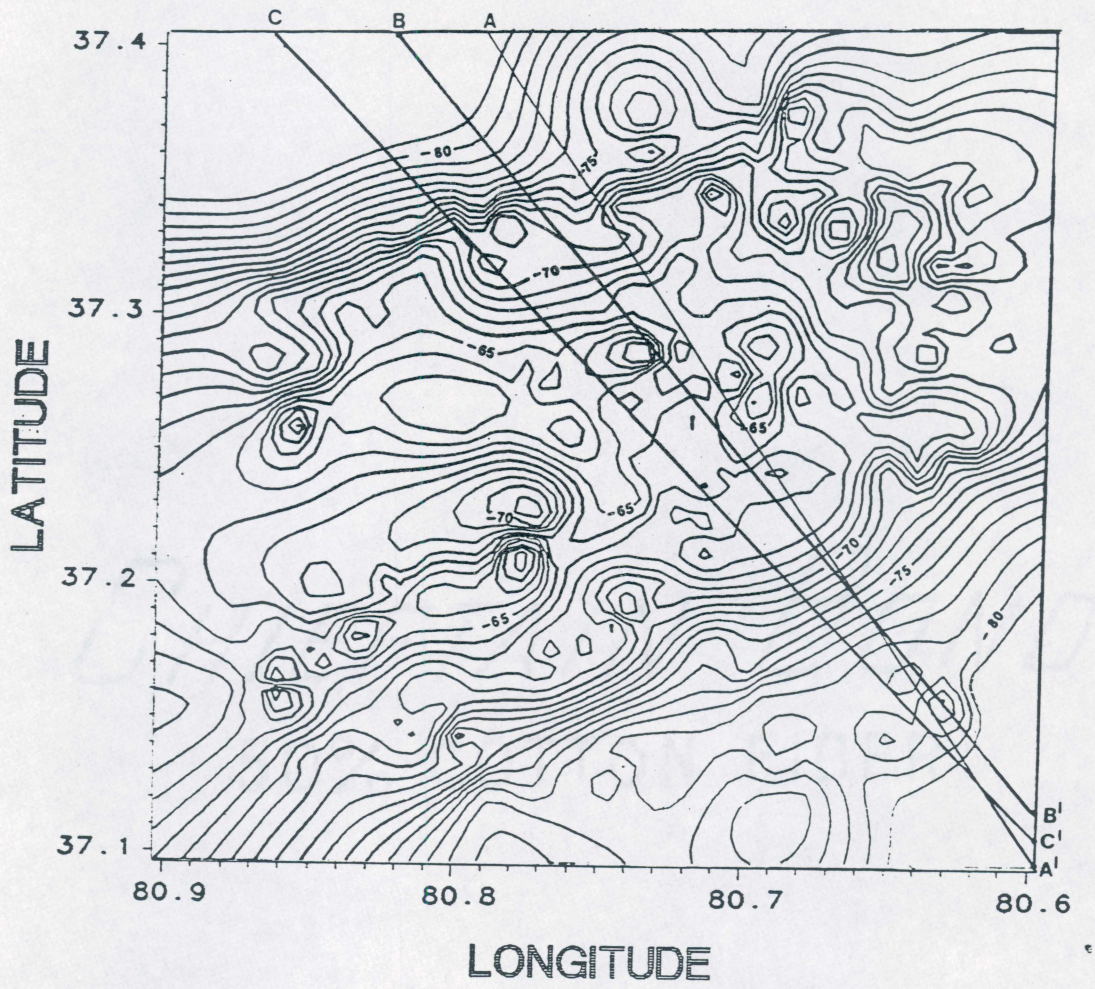

Figure 6. Complete Bouguer Gravity Map: Contour map of complete Bouguer gravity field, contour interval of 1 mgal. Line A-A′ shows location of Gresko cross section, line B-B′ shows location of Woodward and Gray cross section, and line C-C′ shows location of Bartholomew cross section.

Regional Field

One of the initial steps in gravity anomaly analysis is the removal of the regional field. Various arbitrary analytical methods have been developed to accomplish this separation. Such methods as running averages, wavelength filters, and polynomial filters can be used to produce a smoothed gravity field. Other techniques such as upward continuation and field derivatives yield field values on different surfaces which can separate broad from narrow anomaly patterns. One objective of these methods is to separate the anomalies produced from different zones, such as upper crustal, lower crustal, and crust/mantle boundary. But when attempts at the application of arbitrary numerical schemes to gravity data are made it is often difficult to determine their validity. This is because most of these schemes can only discriminate between broad and narrow anomalies and give no information on depths of their sources. Some form of independent information concerning gravity anomaly sources is needed, for example seismic measurements of crustal thickness. From this information the gravity variation related to crustal thickness can be determined.

The complete Bouguer gravity map (Figure 6) indicates the superposition of a broad regional field and a field of local anomalies. For purposes of this study the regional is assumed to result from variations in thickness of the earth's crust. The basis for this assumption is the seismic survey of crustal thickness reported by James, Smith, and Steinhart (1968). Included in their study is a calculated gravity field (Figure 7) that represents the variation in gravity related to crustal thickness.

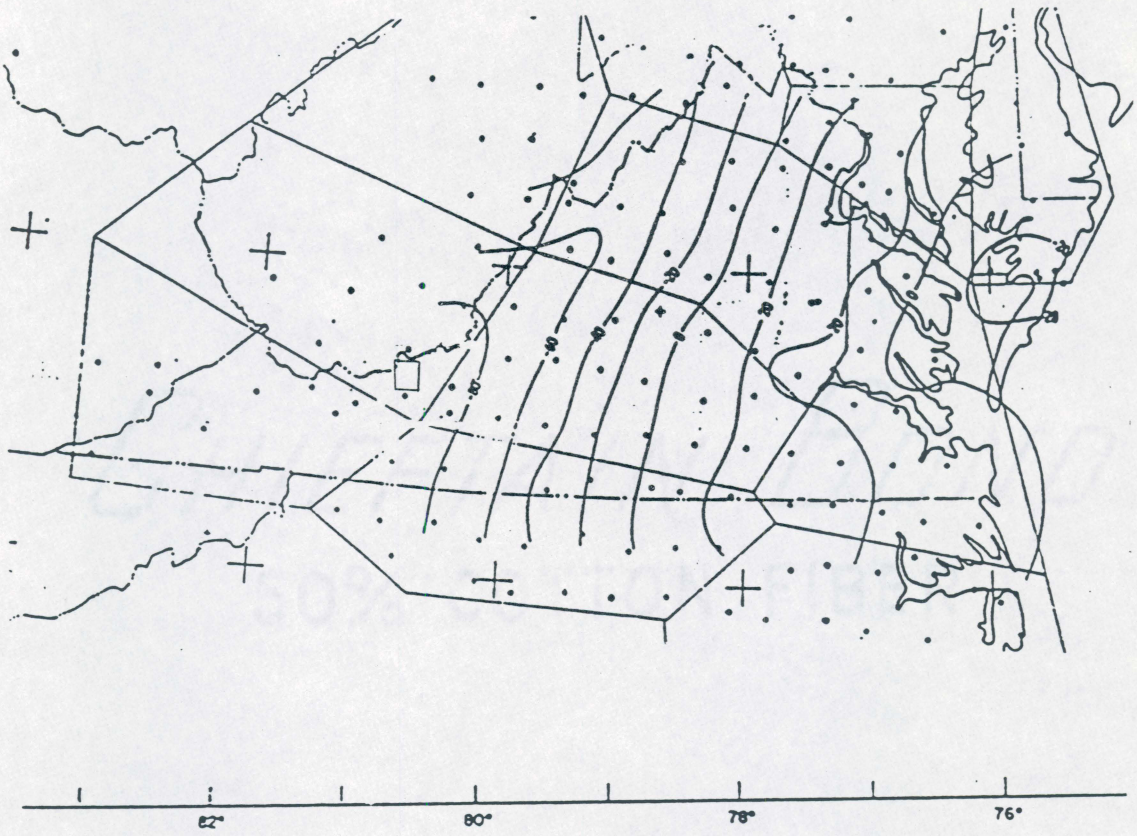

Figure 7. Gravity Field due to Appalachian Crustal Structure: Theoretical gravity field produced by crustal thickness variations found from seismic refraction data (James, Smith, and Steinhart, 1968).

The Bane Dome is situated on the periphery of the area surveyed by James and others (1968) in a region where their calculated gravity field indicates a gradient of approximately 0.3 mgal/km increasing in the direction of N75W. Near the Bane Dome this regional gradient could be closely expressed by a plane polynomial of the form:

$$g_r(X, Y) = AX + BY + C \tag{3}$$

where g_r is the regional gravity value at longitude X and latitude Y (degrees), and A, B, and C are constant coefficients.

Bouguer gravity values obtained in the present study were used to determine the coefficients of a plane polynomial. This was done with a software package prepared at the SAS Institute in Cary, NC. In a two step procedure Bouguer gravity values were first interpolated at points on a square grid by means of a bicubic spline interpolation. Then a plane polynomial function was fitted to the grid values by the method of least squares. The following coefficients were found:

$$A = -17.1434$$

$$B = 4.8570$$

$$C = -1636.4274.$$

By substituting these values into equation 3 an expression for the regional gravity field is obtained. This expression was used to calculate the regional field that is contoured in Figure 8.

This regional field exhibits a gradient of approximately 0.2 mgal/km increasing in the direction of N76W. This gradient is remarkably similar to that calculated independently by James and others (1968) from seismic measurements of crustal thickness. This excellent comparison is the basis for concluding that the plane regional gravity field obtained from gravity measurements over the Bane Dome is produced for the most part by variation in crustal thickness.

Other efforts to separate a regional field from the Bouguer gravity values included fitting a biquadratic polynomial and calculating upward continuations. Patterns of gravity variation resulting from these calculations were too complicated to attribute simply to variation in crustal thick-

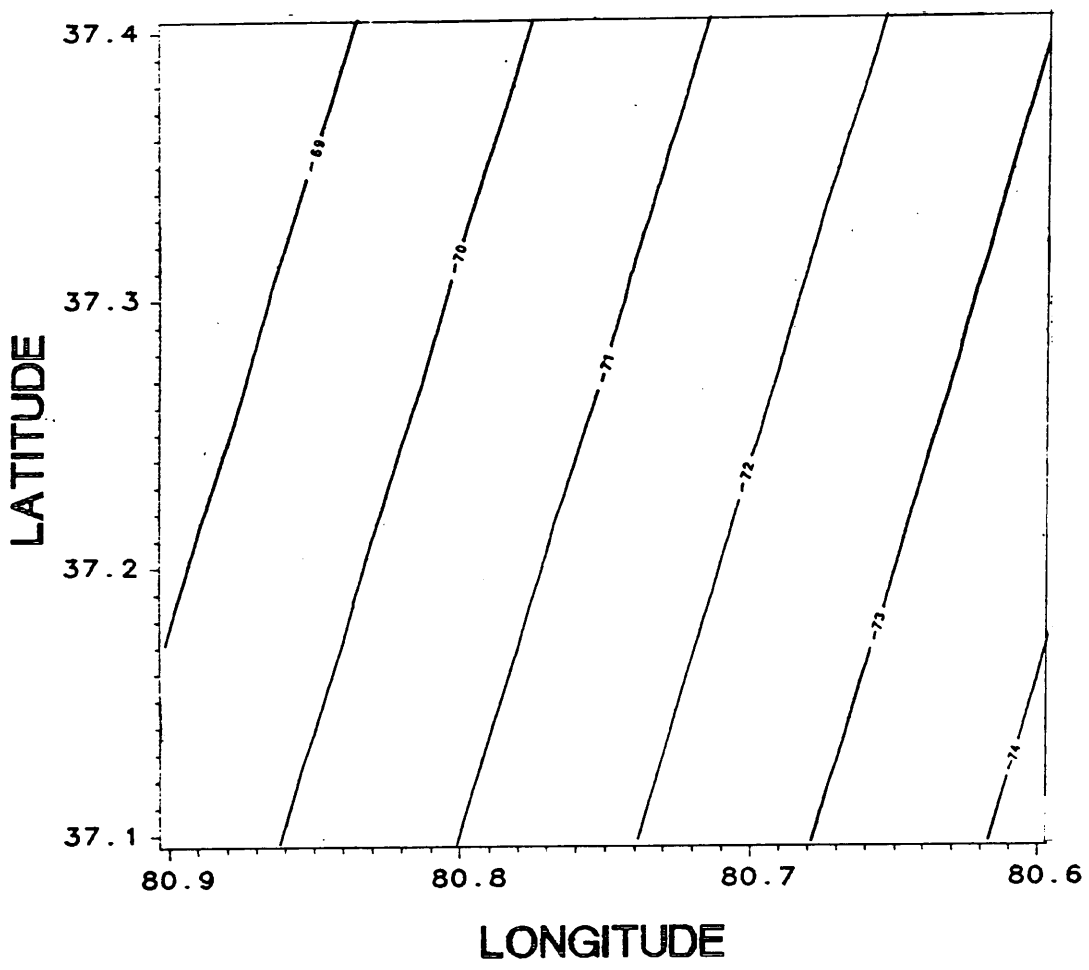

Figure 8. Plane Equation Regional Field: Gravity field expressed by a plane polynomial fitted to Bouguer gravity values by method of least squares. Contour interval is 1 mgal.

ness. It was concluded that these regional fields resulted from combinations of this source and upper crustal anomaly sources.

Upper Crustal Anomaly Sources

The principal purpose of this study is to examine gravity anomalies associated with the Bane Dome. These anomalies can be presented more clearly by subtracting from the Bouguer gravity field (Figure 6) the variation of gravity related to crustal thickness (Figure 8). The result is the residual gravity anomaly map in Figure 9.

The most prominent feature of the residual field in the is the broad gravity high situated directly over the Bane Dome, which has an amplitude of approximately 12 mgal. Otherwise there are several local anomalies that can be attributed mainly to the distribution of high density carbonate rocks of the Knox Group and the Honaker Formation, and the contrasting lower density clastic rocks within the dome. The contacts of these rock units, as mapped by Schultz and others (1986) are included in Figure 9 for qualitative correlation with gravity anomalies. The geologic cross sections in Figure 4 show different interpretations of how these rocks are distributed. These geologic interpretations are tested by comparing residual gravity anomalies observed along these profiles with the theoretical variation of gravity calculated for two dimensional models that conform to these three cross sections.

The residual gravity variation over the geologic cross sections is shown in Figures 10, 11, and 12. Gravity values at contour intersections with the profile lines in Figure 9 were plotted and

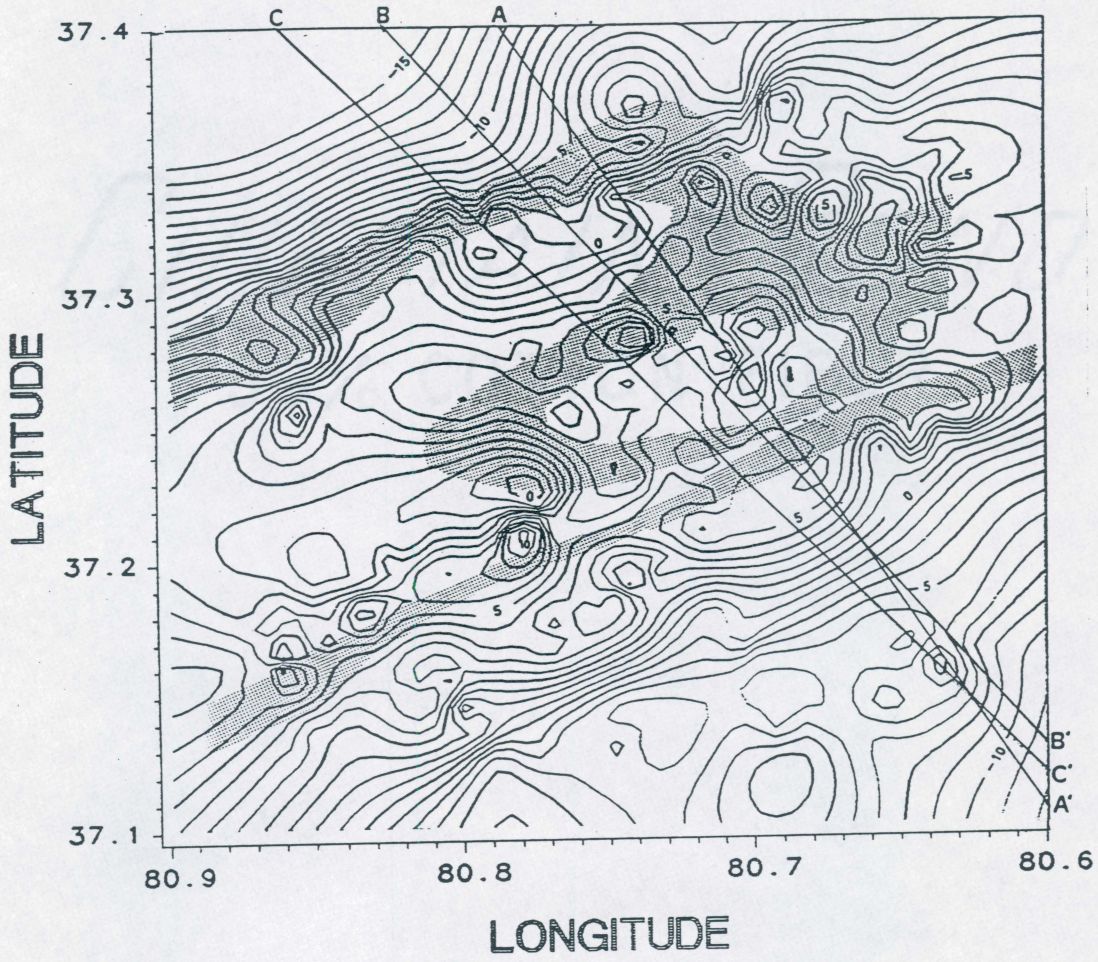

Figure 9. **Upper Crustal Anomaly Pattern:** Residual gravity field obtained by subtracting plane polynomial field (Figure 8) from Bouguer gravity field (Figure 6) field. Stipling indicates outcrops of Knox group (Schultz and others, 1988). Contour interval is 1 mgal. Line A-A′ shows location of Gresko cross section, line B-B′ shows location of Woodward and Gray cross section, and line C-C′ shows location of Bartholomew cross section.

connected by dashed lines. Also, residual gravity values at all points within 1 km were projected to the profile lines and plotted at those locations.

Theoretical variation of gravity over two-dimensional models was calculated by the well known method of Talwani, Worzel, and Landisman (1959). The models were prepared from the geologic cross sections by reading depths to contacts between rock units at 0.25 km intervals along the Gresko (1985) and the Woodward and Gray (Woodward, 1985) profiles, and at 0.40 km intervals along the Bartholomew profile. Density values assigned to the two dimensional model units correspond to values measured by Kolich (1974) and Edsall (1974) for rocks represented by these model units. These two dimensional models and the corresponding theoretical gravity profiles are shown in Figures 10, 11, and 12. Also shown for convenience of comparison are the geologic cross sections of Gresko, Woodward and Gray, and Bartholomew.

The gravity variation predicted by the Gresko model compares favorably with the observed residual anomalies. The broad high of approximately 12 mgal is properly reproduced, and local anomalies of the same character are evident. The average difference between the observed and theoretical gravity profiles is -1.6 mgal, and the standard deviation is 1.9 mgal. Because the actual anomaly sources are of finite dimensions, it is not practical to attempt to reproduce all features by means of a two dimensional model. The results show that the main features and the general character of the theoretical gravity profile are consistent with the observed profile.

The interpretation of Woodward and Gray also predicts a broad gravity high over the Bane Dome. The average departure of the theoretical gravity profile from the observed residual profile is -1.5 mgal, and the standard deviation is 2.1 mgal. The largest departure is over the crest of the dome where the theoretical gravity is between 2 and 3 mgal higher than the residual gravity field. Otherwise, the theoretical gravity profile reproduces the main features of the residual gravity profile.

The gravity profile over the Bartholomew model is seen to be consistent with the principal features of the observed residual gravity profile. The average departure is -0.8 mgal, and the standard deviation is 2.2 mgal. The largest departure occurs near the center of the profile where a local high anomaly is not reproduced by the gravity over the two-dimensional model. This local

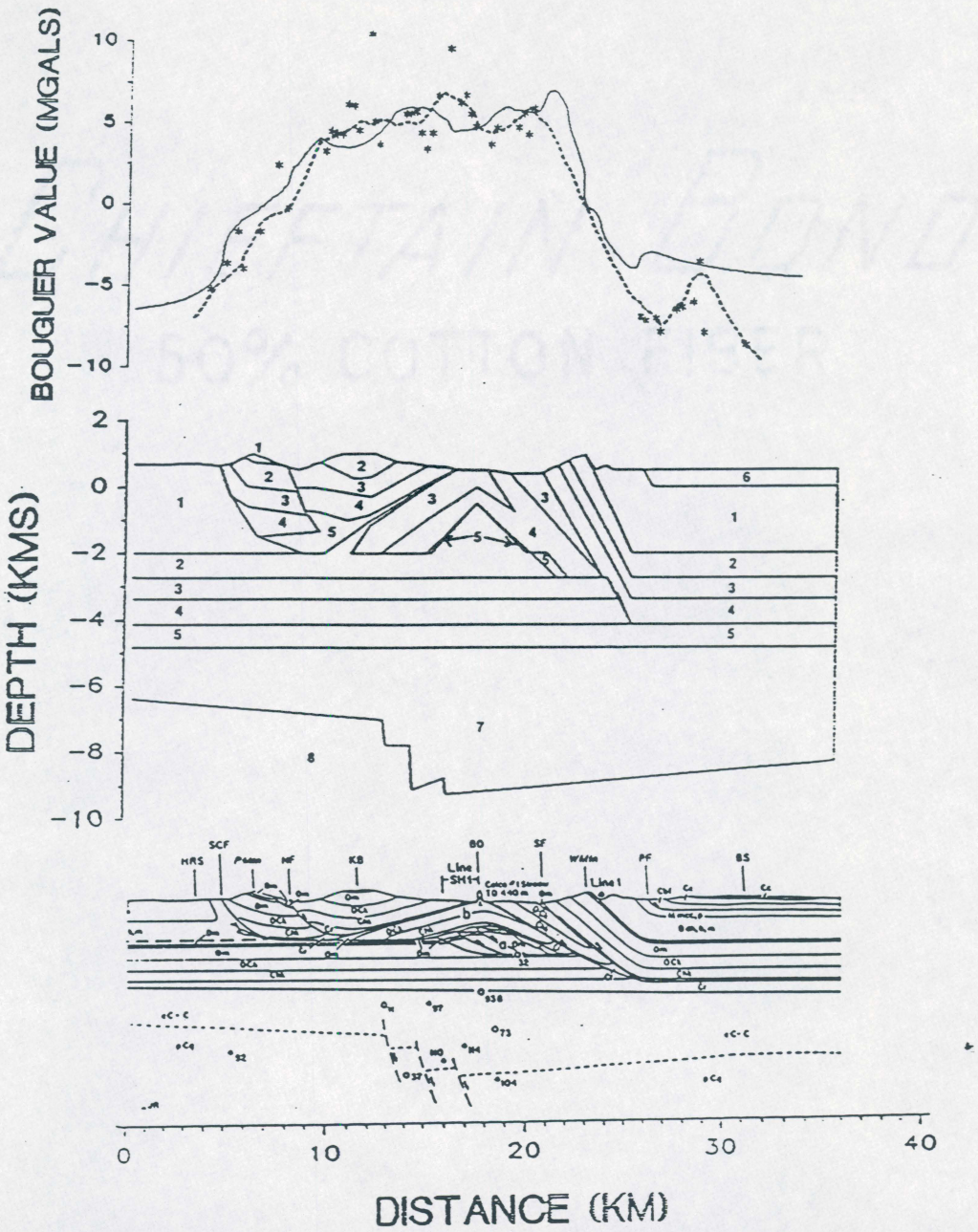

Figure 10. **Gresko Gravity Profile:** Plot of gravity profile over the Gresko model (top) Solid line indicates measured residual gravity anomaly profile, broken line indicates gravity variation computed for digitized model (middle), and stars indicate station gravity measurements within 1 km of profile. Density units used for digitized model are as follows; 1 = 2.67 gm/cc, 2 = 2.70 gm/cc, 3 = 2.80 gm/cc, 4 = 2.85 gm/cc, 5 = 2.67 gm/cc, 6 = 2.80 gm/cc, 7 = 2.73 gm/cc, and 8 = 2.77 gm/cc. Numbers of model units refer to a common density but not common stratigraphic units. Gresko (1985) geologic cross section is also included for comparison with digitized model (bottom). See Figure 4 for formation labels on geologic cross section.

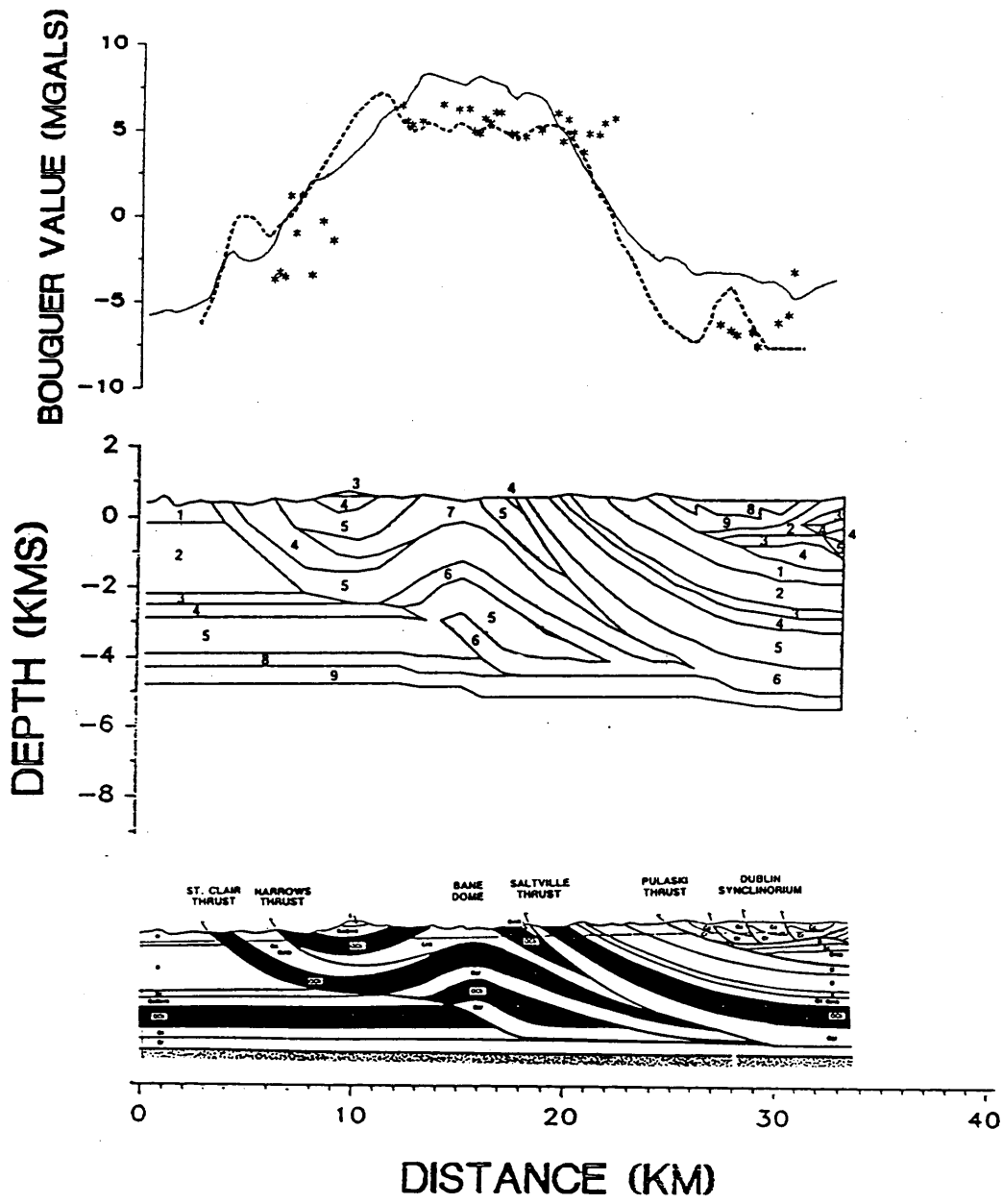

Figure 11. **Woodward and Gray Gravity Profile:** Plot of gravity profile over the Woodward and Gray model (top) Solid line indicates measured local gravity anomaly profile, broken line indicates gravity variation computed for digitized model (middle), and stars indicate station gravity measurements within 1 km of profile. Density units used for digitized model are as follows; 1 = 2.67 gm/cc, 2 = 2.70 gm/cc, 3 = 2.73 gm/cc, 4 = 2.70 gm/cc, 5 = 2.80 gm/cc, 6 = 2.76 gm/cc, 7 = 2.85 gm/cc, 8 = 2.78 gm/cc, and 9 = 2.67 gm/cc. Numbers of model units refer to a common density but not common stratigraphic units. Woodward and Gray (Woodward, 1985) geologic cross section is also included for comparison with digitized model (bottom). See Figure 4 for formation labels on geologic cross section.

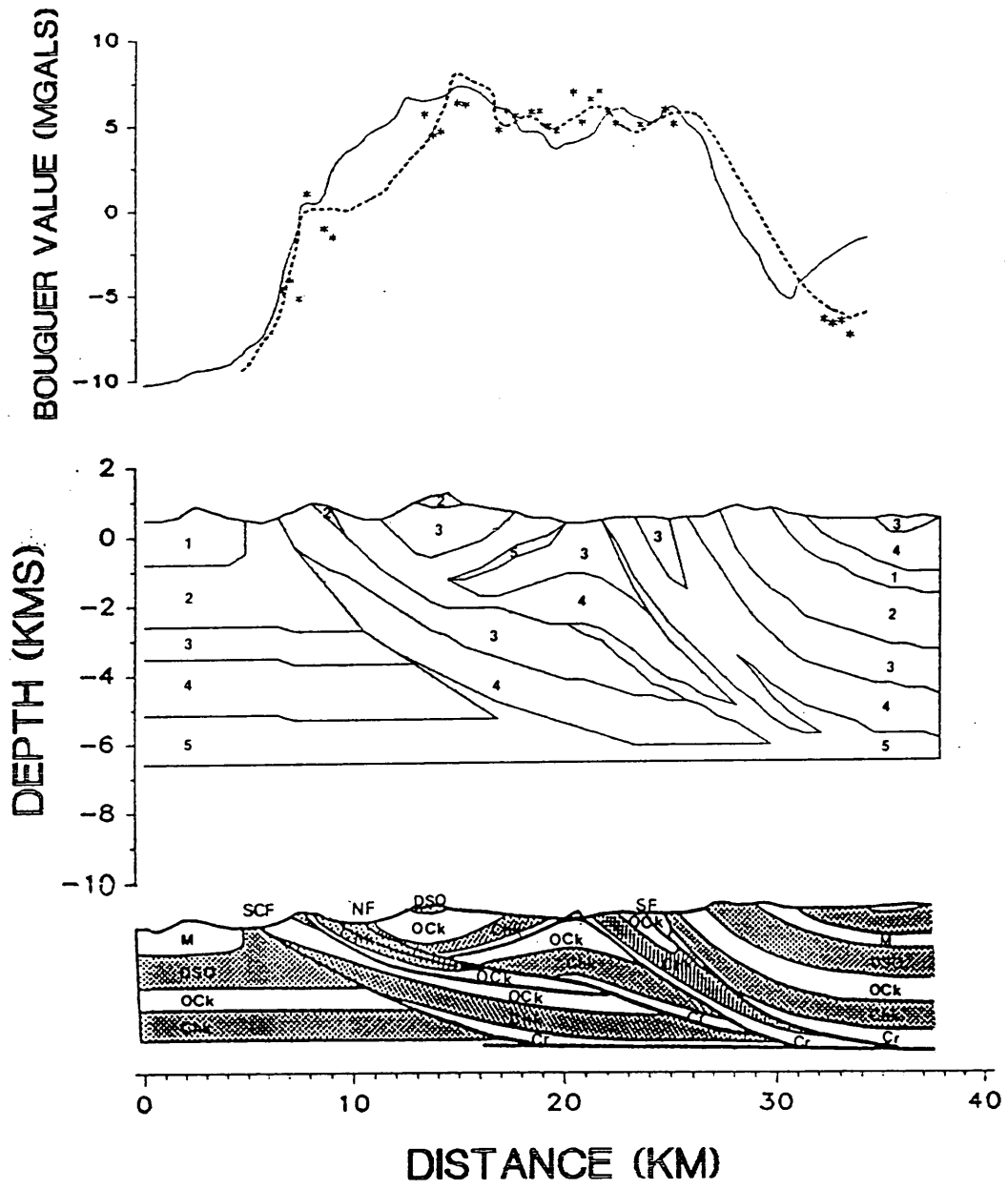

Figure 12. Bartholomew Gravity Profile: Plot of gravity profile over the Bartholomew model (top) Solid line indicates measured local gravity anomaly profile, broken line indicates gravity variation computed for digitized model (middle), and stars indicate station gravity measurements within 1 km of profile. Density units used for digitized model are as follows; 1 = 2.67 gm cc, 2 = 2.70 gm/cc, 3 = 2.80 gm/cc, 4 = 2.85 gm/cc, and 5 = 2.67 gm/cc. Numbers of model units refer to a common density but not common stratigraphic units. Bartholomew (personal communications, 1987) geologic cross section is also included for comparison with digitized model (bottom). See Figure 4 for formation labels on geologic cross section.

high can be attributed to an anomaly source of finite dimensions which is not included on the more general cross section.

The three models used in this study produce similar patterns of gravity variation. Despite the similarities in the general gravity patterns over the models there are some important differences in between the models. The Gresko model shows imbricate thrusts of low density Ordovician Martinsburg Formation at the core of the dome while the other two models show more high density dolomite at the core. The other important difference between the Gresko model and the other models is that the Gresko model is the only one to look below the decollement in the Rome shale. The similarities in the overall character of the gravity variations over the three models indicate that low density rock in the core of the dome coupled with deep basement structure can produce the same overall gravity variations as high density rock in the core and no basement structure. The results in Figures 10, 11, and 12 show that these two contrasting interpretations are consistent with the gravity constraints.

An interesting aspect of the problem of separating the regional field from the Bouguer gravity field is seen by examining the contributions of individual upper crustal anomaly sources. Profiles in Figures 13, 14, and 15 show gravity variations over individual units in the two dimensional models. It is clear that some of these upper crustal units produce very broad gravity anomalies that could be difficult to distinguish from broad anomalies produced by deeper sources. For this reason the arbitrary filtering techniques commonly used to separate the regional field cannot be expected to separate anomalies from deep sources from similarly broad anomalies produced by shallow sources.

In this study a regional field was separated on the basis of independent knowledge of crustal thickness. The residual gravity field remaining after subtraction of that regional field from the Bouguer gravity field can be explained in terms of density contrasts within the upper 10 km of the crust. There is no evidence of anomaly sources deeper in the crust.

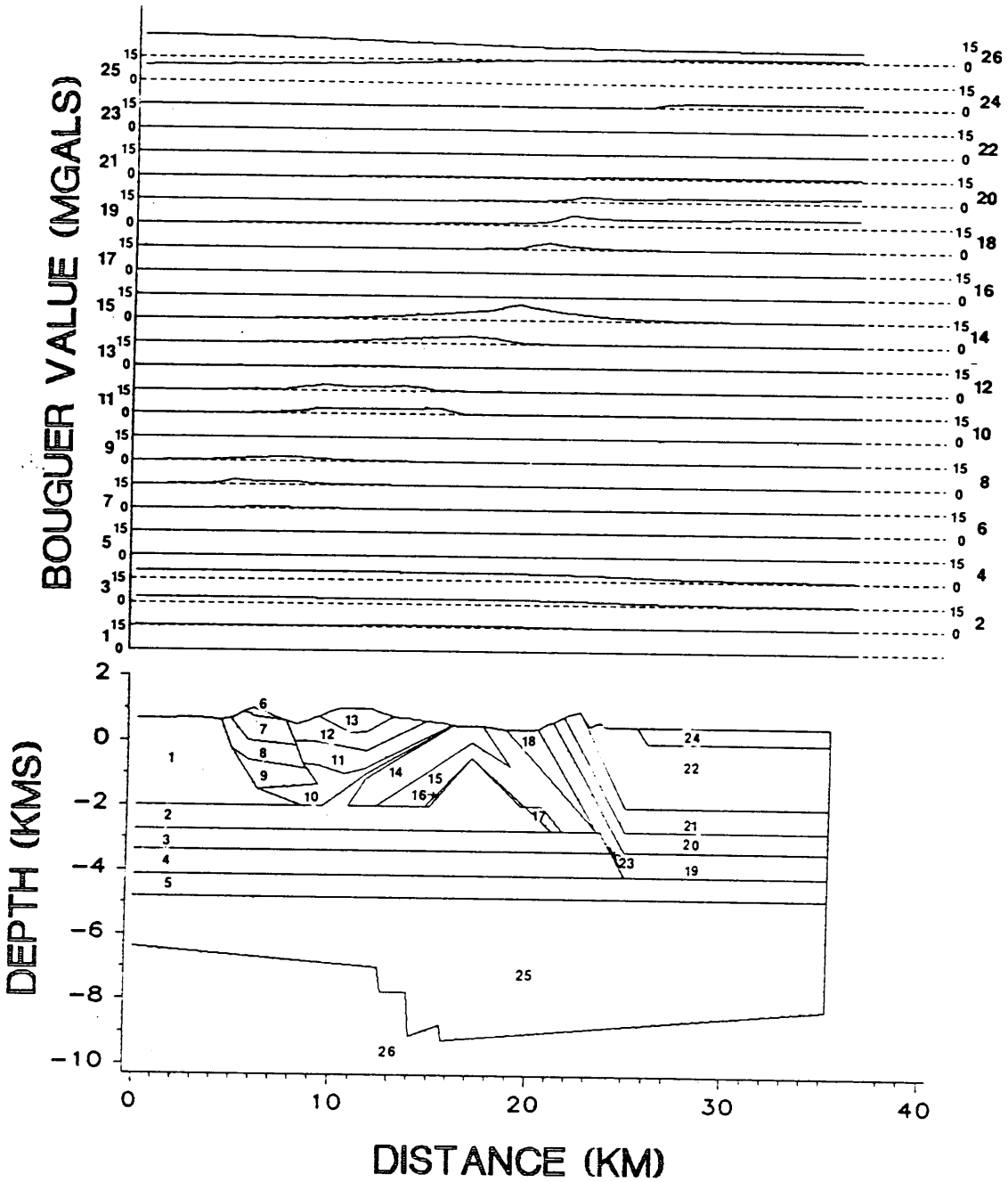

Figure 13. **Contributions to Gresko Gravity Profile:** Theoretical gravity anomalies produced by the individual rock units of the Gresko model. Numbers on digitized cross section correspond to the individual rock units labeled on gravity anomaly source profile.

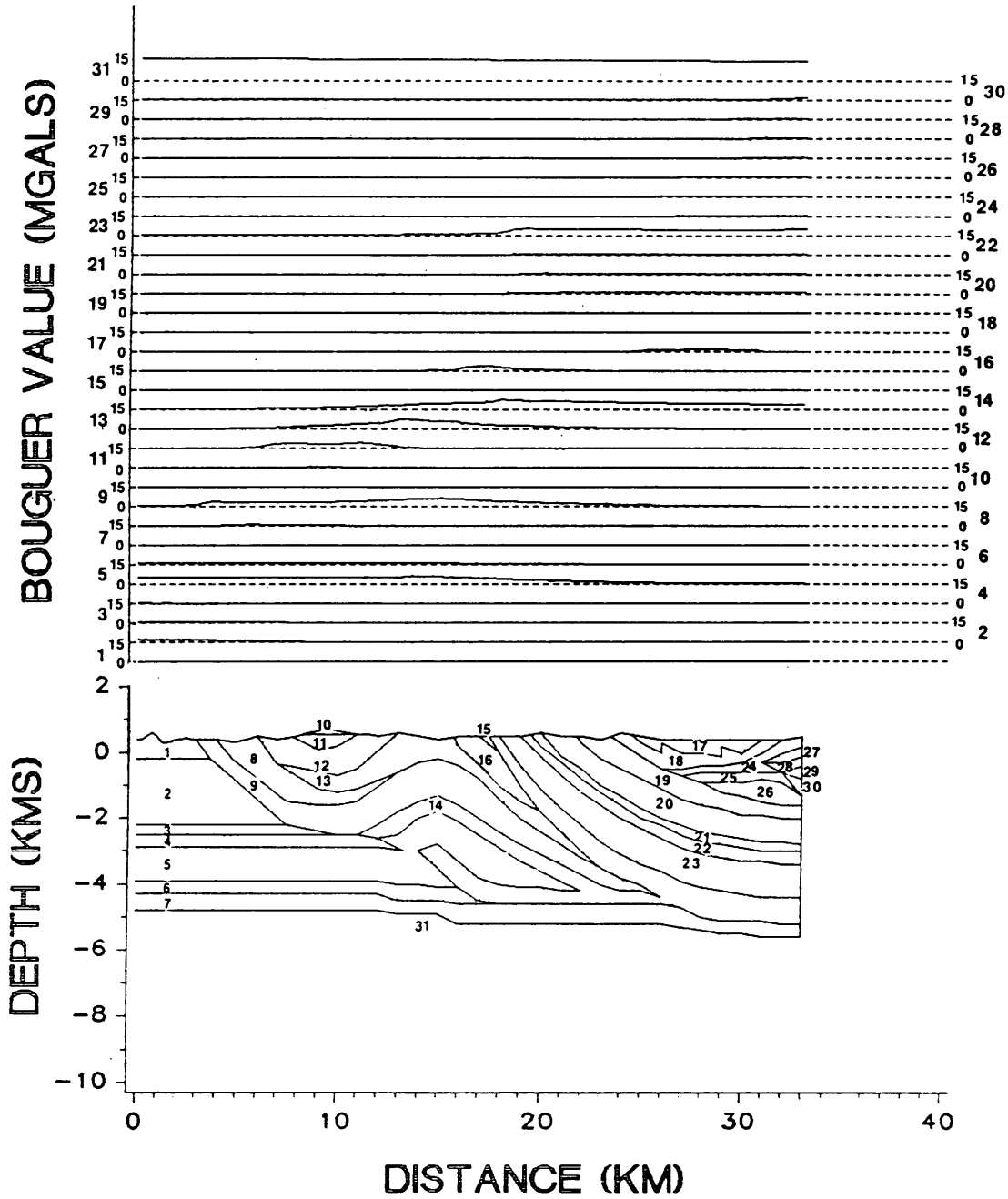

Figure 14. Contributions to Woodward and Gray Gravity Profile: Theoretical gravity anomalies produced by the individual rock units of the Woodward and Gray model. Numbers on digitized cross section correspond to the individual rock units labeled on gravity anomaly source profile.

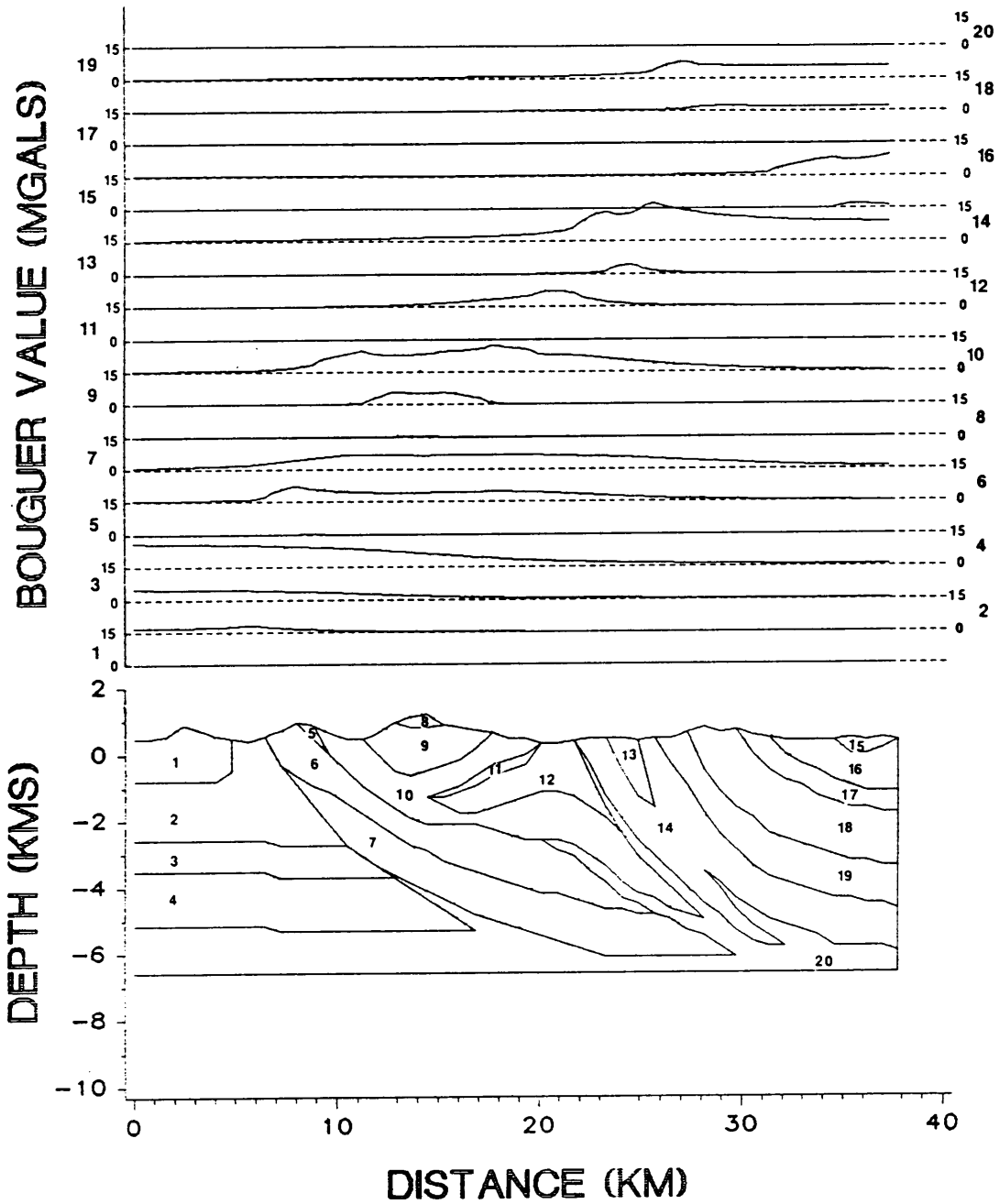

Figure 15. **Contributions to Bartholomew Gravity Profile:** Theoretical gravity anomalies produced by the individual rock units of the Bartholomew model. Numbers on digitized cross section correspond to the individual rock units labeled on gravity anomaly source profile.

Average Density Inversion

Results presented in the previous sections indicate that Bouguer gravity variation in the region of the Bane Dome can be explained in terms of crustal thickness and structure within the upper 10 km of the crust. This conclusion can be tested by means of a density inversion analysis. The idea is to use the gravity measurements to obtain estimates of average density in a zone extending from the land surface to an arbitrary depth T below sea level. Insofar as the average density values are consistent with the densities of rocks known to exist in that zone, it can be concluded that gravity anomalies can be explained by sources within that zone.

A modification of Equation (2) provides the basis for estimating average density values. In that equation the purpose of the term $0.01278\rho h$ is to account for the gravitational attraction of mass extending from sea level up to the height of the gravity station (Robinson and Coruh, 1988). To account for the gravitational attraction of mass in a zone extending from a depth T below sea level to height h of the land surface at the gravity station this term can be replaced by two terms labelled A and B in the following expression:

$$\Delta g_B = g_{obs} - [g_t - 0.09406h - \underbrace{0.01278\rho_0 T}_{A} + \underbrace{0.01278\bar{\rho}(T+h)}_{B} - TC] \qquad (4)$$

where ρ_0 is the density assumed for the outer shell of the normal ellipsoid, and $\overline{\rho}$ is the average density in the zone of the earth reaching from depth T to height h. The purpose of term A is to remove the gravitational attraction of the outer shell of the normal ellipsoid, which extends from its surface to depth T. The purpose of term B is to replace this mass with a plate reaching from depth T below the ellipsoid surface to height h above it. The density of this latter plate can be found by rearranging Equation (4) to obtain:

$$\overline{\rho} = \frac{\Delta g_B - g_{obs} + g_t - 0.09406h - 0.01278\rho_0 T - TC}{0.01278(T+h)} \tag{5}$$

Then by substitution from Equation (1) the expression becomes:

$$\overline{\rho} = \frac{\Delta g_B - \Delta g_{fa} - 0.01278\rho_0 T - TC}{0.01278(T+h)} \tag{6}$$

To the extent that term B in Equation (4) correctly expresses the gravitational attraction of the mass beneath a gravity station the Bouguer gravity at that station should be the same as the Bouguer gravity at all other stations, if all gravity anomaly sources lie above the depth T. Or, if the depth T is chosen so that the zone above it does not contain regional field sources, but does contain all other anomaly sources, then the Bouguer gravity computed for any station using Equation (4) should be the same as the regional gravity Δg_r at that station.

For purposes of this study a standard density of ρ_0 = 2.75 gm/cc was chosen for the zone above the depth T. Then, average density $\overline{\rho}$ was calculated for each gravity station using values of T equal to 0, 2, 4, 6, 8, and 10 km in Equation (6). In each calculation the elevation, free air gravity, and terrain correction at the station were used, and the regional gravity g_r was substituted for Bouguer gravity Δg_B. Maximum values of $\overline{\rho}$, minimum values of $\overline{\rho}$, and the ranges of $\overline{\rho}$ are plotted with the corresponding values of T in Figure 16. Average density values corresponding to T = 10 km are contoured in Figure 17.

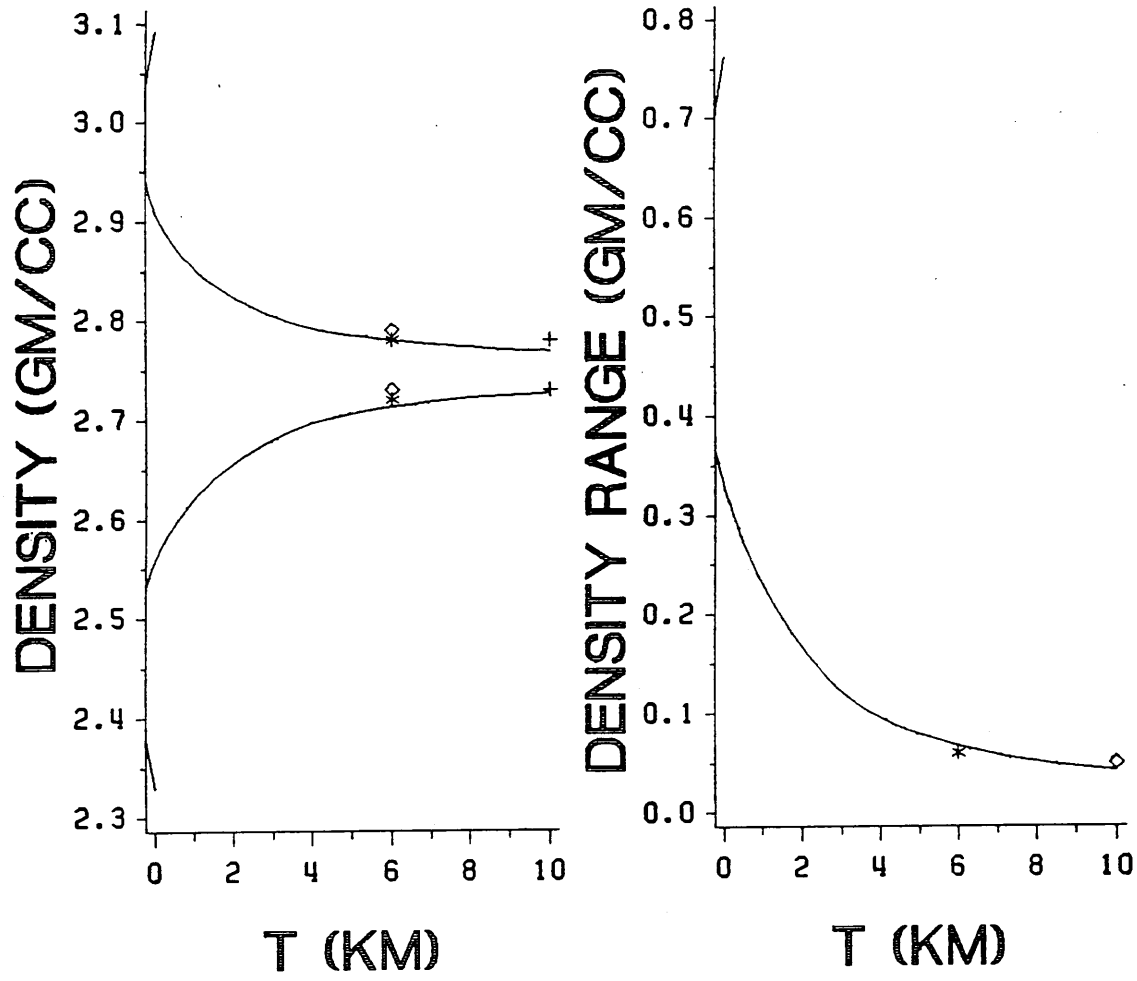

Figure 16. **Average Density Comparisons:** Plots of maximum and minimum density values $\bar{\rho}$ and the range of density values as functions of plate depth (T). Stars indicate values found from Woodward and Gray model, diamonds indicate values found from Bartholomew model, and plusses indicate values found from Gresko model.

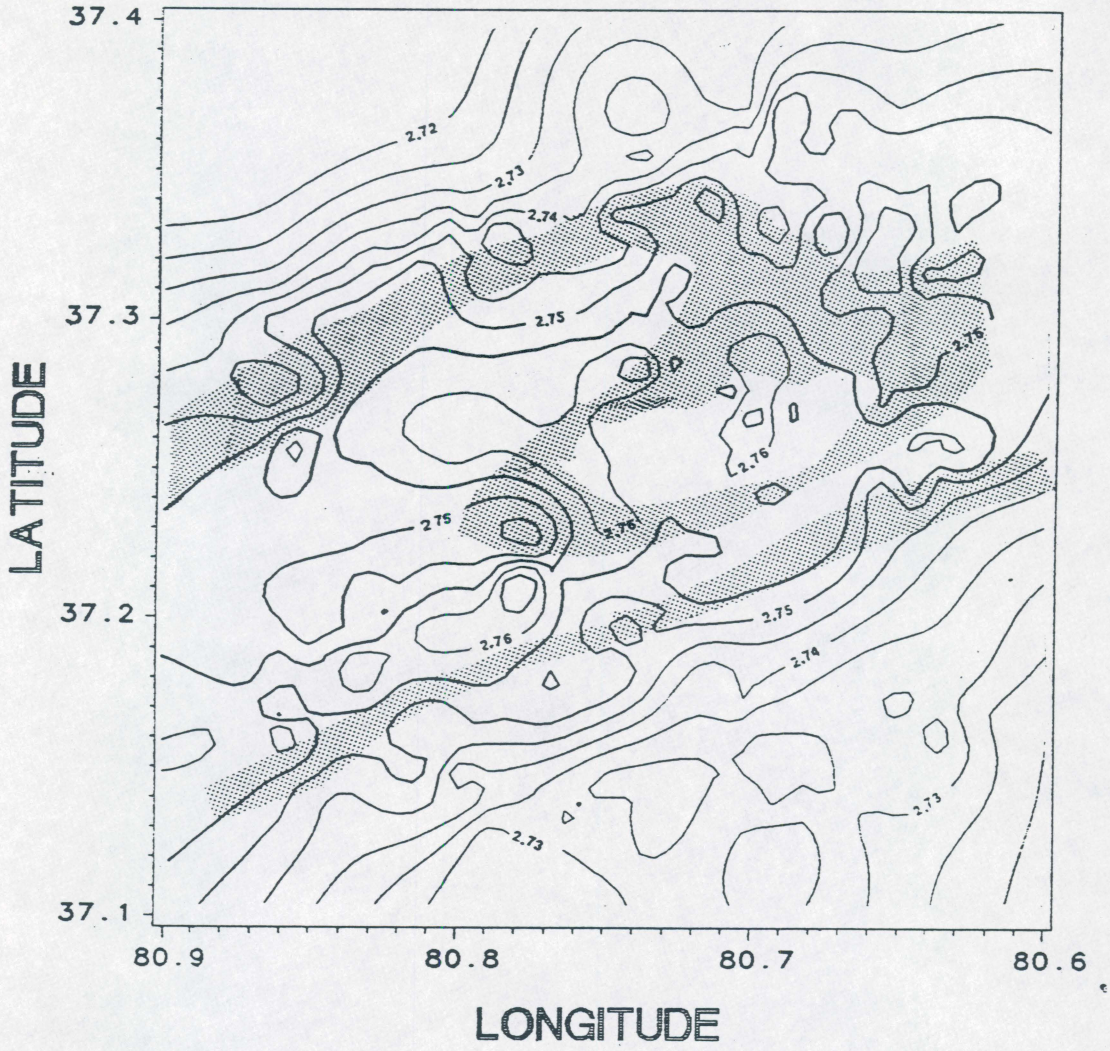

Figure 17. Average Density Contour Map: Contour map of density values $\bar{\rho}$ found for 10 km plate (T = 10) Stipling indicates locations of outcrops of Knox Group. Contour interval of 0.005 gm/cc used to produce map.

Table 2. Average density data for two dimensional models

Model	Maximum $\bar{\rho}$	Minimum $\bar{\rho}$	Range
Woodward and Gray	2.78 gm/cc	2.72 gm/cc	0.06 gm/cc
Bartholomew	2.79 gm/cc	2.73 gm/cc	0.06 gm/cc
Gresko	2.78 gm/cc	2.73 gm/cc	0.05 gm/cc

At points along the profiles in Figures 10, 11, and 12 average density was calculated from the density variation along vertical lines extending down from the land surface to depths below sea level of 6 km for the Woodward and Gray model and the Bartholomew model, and 10 km for the Gresko model. The maximum and minimum values of average density, and the average density ranges for these profiles are given in Table 2, and are plotted in Figure 16.

The average density values and density ranges determined from gravity station data are seen to be comparable with the similar values and ranges found from the two dimensional models. These comparisons confirm the conclusion that the residual gravity field (Figure 8) can be attributed to anomaly sources within the upper 10 km of the crust. Figure 17 shows an estimate of the variation in average density in this zone that is associated with the residual gravity field.

Conclusion

A broad gravity anomaly approximately 12 mgal in amplitude is associated with the Bane Dome. Superposed on this anomaly are several smaller anomalies with amplitudes of a few milligals. For the most part they are produced by the distribution of relatively high density carbonate rocks and lower density clastic rocks within the dome.

Two contrasting interpretations of the structure of the Bane Dome are consistent with constraints imposed by gravity measurements. One interpretation, represented by the geologic cross sections of Woodward and Gray (Woodward, 1985) and Bartholomew (personal communications, 1987) suggests a relative abundance of high density carbonate rocks within the dome transported by overthrusting within the Narrows thrust sheet. Because the gravity anomalies can be entirely explained by sources confined to the Narrows thrust sheet, this interpolation precludes the existence of significant lateral density contrasts associated with deeper structure beneath the decollement zone in the Rome Formation.

The contrasting interpretation represented by the cross section of Gresko (1985), suggests a smaller proportion of carbonate rocks in the Narrows thrust sheet, and more lower density clastic rocks. This interpretation proposes high angle faults with associated lateral density contrasts in the deeper rocks underlying the decollement. Because sources within the Narrows thrust sheet are in-

sufficient to completely account for the gravity anomalies, the density contrasts associated with deeper structure are required.

The Bouguer gravity field can be separated into regional and residual parts. The regional field can be attributed to change in crustal thickness known independently from the seismic measurements of James, Smith, and Steinhart (1968). The remaining residual field can be explained in terms of anomaly sources within the upper 10 km of the crust.

Bibliography

Bartholomew, M. J., 1984. Structural Evolution of a Portion of the Eastern (Appalachian) Overthrust Belt-A New Model. Geol. Soc. Amer. Abs. with Prog., v.16, no.6, p.438.

Bollinger, G. A., Teague, A. G., Munsey, J. W., and Johnston, A. C., 1985. Focal Mechanism Analyses for Virginia and Eastern Tennessee Earthquakes (1978-1984). NUREG/CR-4288, p.83.

Butts, C., 1933. Geologic Map of the Appalachian Valley of Virginia with Explanatory Text. Va. Geol. Survey Bull. 42, 56p.

Cooper, B. N., 1961. Grand Appalachian Excursion. Va. Engr. Exper. Sta. Extens. Ser., Geol. Guidebook 1, 187 p.

Cooper, B. N., 1964. Relation of Stratigraphy to Structure in the Southern Appalachians. In Tectonics of the Southern Appalachians, Virginia Polytechnic Institute and State University Dept. of Geol. Sci. Mem. 1, p.81-114.

Edsall, R. W., 1974. A Seismic Reflection Study over the Bane Anticline in Giles County, Virginia. MS Thesis, Virginia Polytechnic Institute and State University, 111p.

Gresko, M. J., 1985. Analysis and Interpretation of Compressional (P-Wave) and Shear (SH-Wave) Reflection Seismic and Geologic Data over the Bane Dome, Giles County, Virginia. Phd Dissertation, Virginia Polytechnic Institute and State University, 74p.

Hammer, S., 1939. Terrain Corrections for Gravimeter Stations. Geophysics, vol. 4, p.184-194.

James, D. E., Smith, T. J., and Steinhart, J., S., 1968. Crustal Structure of the Middle Atlantic States. Journ. Geophys. Res., vol. 73, no. 6, p.1983-2007.

Kolich, T. M., 1974. Seismic Reflection and Refraction Studies in Folded Valley and Ridge Province at Price Mountain, Montgomery County, Virginia. MS Thesis, Virginia Polytechnic Institute and State University, 139p.

Lewis, S. E., and Bartholomew, M. J., 1984. Development of Classic Dome and Basin Structures within the Eastern (Appalachian) Overthrust Belt. Geol. Soc. Amer. Abs. with Prog., v.16, no.6, p.575.

Longman, I. M., 1959. Formulas for Computing the Tidal Accelerations Due to the Moon and the Sun. Journ. Geophys. Res., vol. 64, no. 12, p.2351-2355.

Mullenax, A. C., 1981. Deformational Features within the Martinsburg Formation in the St. Clair and Narrows Thrust Sheets, Giles County, Virginia. MS Thesis, Virginia Polytechnic Institute and State University, 130p.

Perry, W. G., Harris, A. G., and Harris, L. D., 1979. Conodont-based Reinterpretation of Bane Dome- Structural Reevaluation of Allegheny Frontal Zone. Bull. Amer. Assoc. Pet. Geol., 63, p.647-654.

Robinson, E. S., 1974. A Reconnaisance of Tidal Gravity in Southeastern United States. Journ. Geophys. Res., vol. 79, no. 29, p.4418-4424.

Robinson, E. S., and Coruh, C., 1988. Basic Exploration Geophysics. John Wiley and Sons, N.Y., N.Y., 541p.

Rodgers, J., 1949. Evolution of Thought on Structure of Middle and Southern Appalachians. Bull. Amer. Assoc. Pet. Geol., 33, p.1643-1654.

Schultz, A. P., Stanley, C. B., Gathright, T. M., II, Rader, E. K., Bartholomew, M. J., Lewis, S. E., and Evans, N. H., 1986. Geologic Map of Giles County, Virginia. Va. Div. of Mineral Resources Publication 69.

Sears, C. E. and Robinson, E. S., 1971. Relations of Bouguer Gravity Anomalies to Geological Structure in the New River District of Virginia. Geol. Soc. of Amer. Bull., v.82, p.2631-2638.

Stovall, R. L., Robinson, E. S., and Batholomew, M. C., 1988. Gravity Anomalies and Geology in the Blue Ridge Province Near Floyd, Virginia. Contributions to Virginia Geology, VI, in press.

Talwani, M., Worzel, J. L., and Landisman, 1959. Rapid Gravity Computations for Two-Dimensional Bodies with Application to the Mendocino Submarine Fracture Zone. Journ. Geophys. Res., vol. 64, p.49-59.

Whitman, H. M., 1960. Stratigraphy of Pearisburg Syncline Area, Giles County, Virginia. Unpublished field report, Virginia Polytechnic Institute and State University, 66p.

Woodward, N. B., 1985. Valley and Ridge Thrust Belt: Balanced Structural Sections, Pennsylvania to Alabama. Appalachian Basin Industrial Associates/University of Tennessee Department of Geological Sciences-Studies in Geology 12, 64p.

Woollard, G. P., 1979. The New Gravity System- Changes in International Gravity Base Values and Anomaly Values. Geophysics, vol. 44, no. 8, p.1352-1366.

Appendix A. Gravity Data

Station	Latitude	Longitude	Elevation	Gravity Value	Free Air Anomaly	Bouguer Anomaly	Terrain Corr.	Complete Bouguer Anomaly
10001	37.3336	80.7499	1650.0	979762.75	-14.82	-71.04	2.74	-68.30
10002	37.3313	80.7425	1815.0	979754.25	-7.81	-69.64	0.54	-69.10
10003	37.3264	80.7389	1920.0	979748.19	-3.99	-69.41	0.18	-69.23
10004	37.3279	80.7483	1960.0	979743.81	-4.61	-71.38	0.42	-70.96
10005	37.3223	80.7364	1915.0	979747.75	-3.96	-69.21	0.17	-69.04
10006	37.3268	80.7278	1790.0	979755.44	-8.97	-69.95	1.31	-68.64
10007	37.3201	80.7184	1880.0	979750.44	-4.57	-68.62	0.24	-68.38
10008	37.3262	80.7196	1790.0	979755.37	-9.03	-70.02	2.51	-67.51
10009	37.3197	80.7096	1965.0	979744.56	-2.45	-69.40	0.08	-69.32
10010	37.3265	80.7082	1901.0	979749.31	-4.66	-69.42	0.12	-69.30
10011	37.3207	80.6940	1975.0	979742.81	-3.26	-70.55	0.04	-70.51
10012	37.3221	80.6995	1985.0	979743.12	-2.01	-69.63	0.08	-69.55
10013	37.3283	80.6991	1880.0	979747.62	-8.32	-72.37	0.09	-72.28
10014	37.3296	80.6957	1850.0	979747.87	-10.89	-73.92	0.14	-73.78
11015	37.3348	80.6882	1855.0	979750.75	-7.54	-70.74	0.30	-70.44
11016	37.3391	80.6836	1810.0	979752.81	-10.65	-72.32	0.64	-71.68
11017	37.3347	80.6791	1655.0	979762.00	-15.10	-71.49	3.79	-67.70
11018	37.3270	80.6751	1765.0	979757.12	-9.63	-69.77	3.55	-66.22
11019	37.3323	80.6748	1655.0	979762.19	-14.92	-71.30	3.66	-67.64
11020	37.3363	80.6696	1780.0	979754.37	-11.91	-72.55	3.75	-68.80
11021	37.3404	80.6644	1800.0	979749.25	-15.16	-76.48	3.86	-72.62
11022	37.3469	80.6630	2000.0	979741.31	-5.22	-73.36	3.82	-69.54
11023	37.3511	80.6593	2170.0	979732.19	1.64	-72.29	3.73	-68.56
11024	37.3567	80.6624	2190.0	979731.19	2.52	-72.09	3.72	-68.37
11025	37.3620	80.6642	2050.0	979739.50	-3.27	-73.11	3.87	-69.24
11026	37.3683	80.6557	2475.0	979713.00	9.33	-75.00	3.57	-71.43
11027	37.3642	80.6552	2395.0	979718.44	8.11	-73.48	3.25	-70.23
11028	37.3322	80.7300	1790.0	979755.31	-9.10	-70.08	1.77	-68.31
11029	37.3372	80.7219	1870.0	979753.69	-4.13	-67.84	0.09	-67.75
11030	37.3596	80.7057	1650.0	979762.62	-17.76	-73.98	1.60	-72.38
11031	37.3560	80.7033	1720.0	979758.19	-14.68	-73.28	1.03	-72.25
11032	37.3527	80.7049	1795.0	979754.87	-10.94	-72.09	0.74	-71.35
11033	37.3499	80.7097	1945.0	979748.69	-3.02	-69.28	0.19	-69.09
11034	37.3442	80.7132	1876.0	979751.37	-5.88	-69.80	0.15	-69.65
11035	37.3397	80.7188	1840.0	979758.94	-1.71	-64.39	0.10	-64.29
11036	37.3213	80.6656	1835.0	979747.81	-11.43	-73.94	0.24	-73.70
11037	37.3196	80.6552	1800.0	979750.75	-11.78	-73.10	0.19	-72.91
11038	37.3185	80.6472	1725.0	979757.69	-11.90	-70.67	0.73	-69.94
11039	37.3194	80.6384	1655.0	979760.00	-16.17	-72.55	2.64	-69.91
12040	37.3651	80.7092	1890.0	979747.19	-10.63	-75.02	1.39	-73.63
12041	37.3666	80.7040	1945.0	979743.75	-8.89	-75.16	0.67	-74.49
12042	37.3718	80.7015	1940.0	979744.25	-9.74	-75.83	1.06	-74.77
12043	37.3692	80.6941	1955.0	979751.31	-1.27	-67.87	0.97	-66.90
12044	37.3685	80.6838	1943.0	979745.87	-7.83	-74.03	3.81	-70.22
12045	37.3714	80.6680	1835.0	979752.25	-11.61	-74.13	3.86	-70.27
12046	37.3724	80.6728	1730.0	979758.50	-15.24	-74.18	3.89	-70.29
12047	37.3668	80.6729	1775.0	979756.31	-12.32	-72.79	3.81	-68.98
12048	37.3620	80.6802	1670.0	979761.19	-17.32	-74.21	3.67	-70.54
12049	37.3578	80.6826	1665.0	979761.62	-17.35	-74.08	2.91	-71.17
12050	37.3526	80.6937	1605.0	979767.00	-16.68	-71.36	2.93	-68.43

Station	Latitude	Longitude	Elevation	Gravity Value	Free Air Anomaly	Bouguer Anomaly	Terrain Corr.	Complete Bouguer Anomaly
12051	37.3509	80.6992	1595.0	979766.31	-18.31	-72.65	2.87	-69.78
12052	37.3510	80.6827	1790.0	979756.31	-9.97	-70.95	2.72	-68.23
12053	37.3408	80.6725	1805.0	979752.87	-11.06	-72.55	3.12	-69.43
12054	37.3255	80.6275	1845.0	979750.50	-8.74	-71.59	1.77	-69.82
12055	37.3257	80.6381	1700.0	979757.25	-15.62	-73.54	3.97	-69.57
12056	37.3322	80.6352	1770.0	979754.62	-11.66	-71.97	3.85	-68.12
12057	37.3361	80.6323	1819.0	979752.50	-10.12	-72.09	3.77	-68.32
12058	37.3398	80.6295	1915.0	979747.44	-6.15	-71.39	3.65	-67.74
12059	37.3533	80.6408	2540.0	979710.81	15.06	-71.47	3.18	-68.29
12060	37.3480	80.6387	2435.0	979717.00	11.38	-71.58	1.25	-70.33
12061	37.3410	80.6364	2090.0	979736.81	-0.32	-71.52	3.74	-67.78
12062	37.3319	80.6505	1945.0	979742.19	-7.64	-73.91	0.85	-73.06
12063	37.3420	80.6437	2170.0	979732.19	2.58	-71.35	1.09	-70.26
12064	37.3443	80.6558	1923.0	979746.06	-6.77	-72.29	2.97	-69.32
13065	37.3146	80.6363	1680.0	979759.94	-13.88	-71.11	3.46	-67.65
13066	37.3125	80.6315	1775.0	979754.25	-9.69	-70.17	1.13	-69.04
13067	37.3071	80.6393	1830.0	979749.31	-9.46	-71.81	0.11	-71.70
13068	37.3139	80.6453	1675.0	979760.50	-12.85	-69.91	2.27	-67.64
13069	37.3108	80.6557	1860.0	979745.56	-10.39	-73.76	0.06	-73.70
13070	37.3050	80.6597	1740.0	979755.00	-12.24	-71.52	0.40	-71.12
13071	37.3133	80.6744	1745.0	979754.81	-11.95	-71.40	0.24	-71.16
13072	37.3073	80.6656	1930.0	979742.94	-6.43	-72.18	0.07	-72.11
13073	37.2989	80.6652	1820.0	979750.25	-8.52	-70.53	1.43	-69.10
13074	37.3004	80.6543	1810.0	979750.19	-9.53	-71.19	0.14	-71.05
13075	37.2964	80.6489	1955.0	979740.94	-5.14	-71.75	0.05	-71.70
13076	37.3203	80.6301	1695.0	979758.69	-13.72	-71.46	3.40	-68.06
13077	37.3050	80.6462	1625.0	979761.31	-16.74	-72.10	0.69	-71.41
13078	37.2909	80.6285	1810.0	979749.69	-9.09	-70.75	0.28	-70.47
13079	37.2895	80.6341	1920.0	979742.75	-5.68	-71.09	0.12	-70.97
13080	37.2909	80.6465	2220.0	979724.94	4.72	-70.91	0.29	-70.62
13081	37.2890	80.6559	2105.0	979731.69	0.65	-71.06	0.04	-71.02
13082	37.2912	80.6644	2115.0	979732.25	2.16	-69.90	0.03	-69.87
13083	37.2920	80.6755	2165.0	979729.50	4.11	-69.65	0.04	-69.61
13084	37.2919	80.6830	2120.0	979732.87	3.25	-68.97	0.03	-68.94
13085	37.2930	80.6928	1965.0	979744.12	-1.01	-67.96	2.33	-65.63
13086	37.2965	80.7000	1840.0	979750.56	-6.33	-69.02	3.25	-65.77
13087	37.2935	80.7077	1655.0	979760.81	-13.48	-69.86	3.75	-66.11
13088	37.2896	80.7053	1650.0	979761.75	-12.07	-68.29	3.78	-64.51
13089	37.2848	80.7050	1695.0	979759.75	-9.84	-67.59	4.30	-63.29
13090	37.2750	80.7093	1830.0	979750.06	-5.90	-68.24	0.08	-68.16
13091	37.2683	80.7118	1690.0	979758.19	-10.00	-67.58	0.38	-67.20
14092	37.3184	80.7312	1855.0	979752.12	-5.23	-68.43	1.56	-66.87
14093	37.3109	80.7290	1875.0	979751.12	-3.41	-67.29	1.05	-66.24
14094	37.3062	80.7256	2065.0	979739.37	2.70	-67.65	0.06	-67.59
14095	37.3063	80.7106	1990.0	979743.81	0.09	-67.71	0.03	-67.68
14096	37.3104	80.7385	2070.0	979738.81	2.61	-67.91	0.19	-67.72
14097	37.3037	80.7459	2275.0	979727.94	11.02	-66.49	0.32	-66.17
14098	37.3047	80.7383	2020.0	979742.87	1.97	-66.85	0.19	-66.66
14099	37.3000	80.7395	2075.0	979738.62	3.83	-66.86	0.17	-66.69
14100	37.2971	80.7311	1950.0	979746.25	-0.30	-66.73	0.11	-66.62

Station	Latitude	Longitude	Elevation	Gravity Value	Free Air Anomaly	Bouguer Anomaly	Terrain Corr.	Complete Bouguer Anomaly
14101	37.2955	80.7223	1805.0	979754.31	-5.87	-67.37	0.18	-67.19
14102	37.2962	80.7135	1720.0	979758.50	-9.68	-68.28	2.19	-66.09
15103	37.2636	80.7491	1831.0	979750.81	-4.11	-66.49	0.36	-66.13
15104	37.2630	80.7399	1795.0	979753.44	-4.87	-66.03	0.21	-65.82
15105	37.2671	80.7288	1755.0	979755.94	-6.14	-65.93	0.17	-65.76
15106	37.2665	80.7203	1730.0	979757.31	-7.11	-66.05	0.30	-65.75
15107	37.2626	80.7229	1755.0	979754.44	-7.64	-67.43	0.40	-67.03
15108	37.2586	80.7283	1785.0	979752.31	-6.00	-66.82	0.16	-66.66
15109	37.2556	80.7337	1855.0	979748.12	-3.61	-66.81	0.27	-66.54
15110	37.2538	80.7408	1886.0	979745.94	-2.88	-67.13	1.92	-65.21
15111	37.2673	80.7443	1964.0	979742.87	0.46	-66.46	0.13	-66.33
15112	37.2704	80.7396	1935.0	979745.50	0.35	-65.57	0.07	-65.50
15113	37.2545	80.7090	1695.0	979754.87	-11.90	-69.65	4.21	-65.44
15114	37.2614	80.7127	1695.0	979756.31	-11.40	-69.15	4.24	-64.91
15115	37.2738	80.7210	1785.0	979753.50	-6.69	-67.50	1.69	-65.81
15116	37.2742	80.7382	1841.0	979750.50	-4.42	-67.15	0.53	-66.62
15117	37.2817	80.7396	2145.0	979738.69	12.35	-60.72	0.10	-60.62
15118	37.2526	80.6802	1880.0	979742.81	-6.57	-70.62	3.88	-66.74
15119	37.2556	80.6745	1925.0	979739.56	-5.59	-71.17	3.19	-67.98
15120	37.2602	80.6659	2035.0	979733.81	-0.99	-70.32	3.75	-66.57
15121	37.2633	80.6574	2075.0	979732.44	0.46	-70.24	2.45	-67.79
15122	37.2667	80.6579	2018.0	979735.81	-1.53	-70.28	0.38	-69.90
15123	37.2658	80.6624	2010.0	979736.56	-1.53	-70.01	0.39	-69.62
15124	37.2664	80.6750	1860.0	979745.12	-7.07	-70.44	3.91	-66.53
15125	37.2642	80.6845	1775.0	979750.56	-9.63	-70.10	2.27	-67.83
15126	37.2660	80.6865	1745.0	979752.12	-10.89	-70.34	2.12	-68.22
15127	37.2681	80.6932	1695.0	979754.56	-13.15	-70.90	3.07	-67.83
15128	37.2757	80.6901	1665.0	979758.31	-13.16	-69.89	3.31	-66.58
15129	37.2777	80.6826	1710.0	979756.06	-11.18	-69.44	2.78	-66.66
15130	37.2790	80.6756	1755.0	979752.87	-10.14	-69.93	2.32	-67.61
15131	37.2808	80.6718	1780.0	979751.31	-9.35	-69.99	2.21	-67.78
15132	37.2855	80.6638	1870.0	979745.50	-7.63	-71.34	1.09	-70.25
15133	37.2755	80.6541	1970.0	979739.12	-3.67	-70.78	0.35	-70.43
15134	37.2821	80.6460	1885.0	979742.94	-8.79	-73.01	0.13	-72.88
15135	37.2817	80.6392	1837.0	979747.00	-8.30	-70.89	0.73	-70.16
15136	37.2785	80.6300	1790.0	979749.25	-10.47	-71.45	0.50	-70.95
15137	37.2837	80.6266	1755.0	979752.06	-11.89	-71.68	1.68	-70.00
16138	37.3625	80.7152	1925.0	979746.00	-8.52	-74.11	0.56	-73.55
16139	37.3577	80.7190	1795.0	979754.37	-12.38	-73.53	0.61	-72.92
16140	37.3512	80.7209	1665.0	979762.44	-15.60	-72.33	1.02	-71.31
16141	37.3474	80.7265	1615.0	979766.37	-16.37	-71.39	1.67	-69.72
16142	37.3431	80.7314	1595.0	979766.69	-17.00	-71.34	1.72	-69.62
16143	37.3400	80.7381	1595.0	979767.00	-16.68	-71.02	1.77	-69.25
16144	37.3453	80.7442	1575.0	979765.06	-20.50	-74.16	1.34	-72.82
16145	37.3491	80.7412	1630.0	979761.75	-19.58	-75.11	1.03	-74.08
16146	37.3528	80.7447	1755.0	979753.00	-16.57	-76.37	1.00	-75.37
16147	37.3559	80.7412	1755.0	979751.94	-17.64	-77.43	1.18	-76.25
16148	37.3630	80.7426	2005.0	979738.94	-8.06	-76.37	4.42	-71.95
16149	37.3642	80.7461	2090.0	979734.25	-4.76	-75.96	3.90	-72.06
16150	37.2988	80.7464	2199.0	979731.37	8.24	-66.67	0.25	-66.42

Station	Latitude	Longitude	Elevation	Gravity Value	Free Air Anomaly	Bouguer Anomaly	Terrain Corr.	Complete Bouguer Anomaly
16151	37.2922	80.7458	2041.0	979741.56	4.51	-65.02	0.22	-64.80
16152	37.2903	80.7414	2005.0	979743.62	3.19	-65.12	0.17	-64.95
16153	37.2853	80.7309	1950.0	979744.31	-1.30	-67.73	0.21	-67.52
16154	37.2884	80.7288	1835.0	979751.56	-4.86	-67.38	1.24	-66.14
16155	37.2676	80.7024	1785.0	979757.44	-1.82	-62.63	0.45	-62.18
16156	37.2687	80.6518	1970.0	979739.94	-1.92	-69.03	0.44	-68.59
17157	37.2694	80.8738	3615.0	979641.50	54.35	-68.81	0.32	-68.49
17158	37.2731	80.8653	3635.0	979638.69	52.48	-71.36	0.35	-71.01
17159	37.2762	80.8536	3545.0	979645.25	50.58	-70.19	0.31	-69.88
17160	37.2760	80.8488	3525.0	979647.06	50.51	-69.58	0.31	-69.27
17161	37.2708	80.8410	3453.0	979655.12	52.74	-64.90	0.36	-64.54
17162	37.2941	80.7543	2218.0	979730.06	8.72	-66.85	0.34	-66.51
17163	37.2895	80.7617	2278.0	979726.81	12.05	-65.56	0.39	-65.17
17164	37.2868	80.7676	2177.0	979732.56	8.30	-65.87	0.56	-65.31
17165	37.2826	80.7734	2110.0	979736.62	6.06	-65.82	0.79	-65.03
17166	37.2799	80.7788	2148.0	979734.56	8.51	-64.67	0.63	-64.04
17167	37.2757	80.7823	2195.0	979731.69	10.06	-64.73	0.58	-64.15
17168	37.2716	80.7864	2205.0	979731.12	10.43	-64.69	0.44	-64.25
17169	37.2689	80.7890	2205.0	979731.62	11.87	-63.25	0.43	-62.82
17170	37.2664	80.7957	2215.0	979731.19	12.37	-63.09	0.54	-62.55
17171	37.2627	80.7956	2235.0	979730.00	13.07	-63.08	0.45	-62.63
17172	37.2565	80.7997	2161.0	979733.44	10.48	-63.14	0.82	-62.32
17173	37.2527	80.7870	2035.0	979738.94	4.13	-65.20	0.79	-64.41
17174	37.2551	80.7818	2005.0	979740.94	3.31	-65.00	1.50	-63.50
17175	37.2518	80.7722	1940.0	979744.87	1.14	-64.96	1.50	-63.46
17176	37.2544	80.7644	1896.0	979747.50	-0.38	-64.97	2.86	-62.11
17177	37.2581	80.7566	1864.0	979749.19	-1.70	-65.20	0.50	-64.70
17178	37.2692	80.7550	1890.0	979748.12	-1.25	-65.64	0.92	-64.72
17179	37.2714	80.7637	1982.0	979744.44	2.77	-64.75	0.49	-64.26
17180	37.2721	80.7748	2243.0	979727.94	10.82	-65.60	0.25	-65.35
17181	37.2739	80.7786	2295.0	979726.69	14.46	-63.73	0.31	-63.42
18182	37.2559	80.8622	3210.0	979668.50	44.20	-65.16	1.69	-63.47
19183	37.3004	80.8635	1650.0	979758.81	-15.95	-72.16	3.31	-68.85
19184	37.2956	80.8640	1635.0	979759.50	-16.67	-72.38	3.27	-69.11
19185	37.3041	80.8536	1612.0	979761.87	-17.40	-72.32	3.20	-69.12
19186	37.3070	80.8477	1615.0	979761.50	-17.49	-72.51	3.18	-69.33
19187	37.3002	80.8423	1820.0	979751.56	-7.21	-69.22	2.77	-66.45
19188	37.2940	80.8383	2085.0	979737.06	3.21	-67.82	2.51	-65.31
19189	37.2951	80.8304	2175.0	979730.56	5.17	-68.93	2.34	-66.59
19190	37.2994	80.8267	2122.0	979734.56	4.19	-68.10	2.31	-65.79
19191	37.3145	80.8397	1585.0	979762.25	-20.50	-74.50	3.42	-71.08
19192	37.3180	80.8320	1570.0	979763.69	-20.47	-73.96	3.45	-70.51
19193	37.3097	80.8616	1765.0	979750.62	-14.26	-74.39	1.00	-73.39
19194	37.3146	80.8486	1590.0	979761.06	-21.22	-75.39	2.90	-72.49
19195	37.3203	80.8304	1545.0	979764.50	-22.01	-74.65	3.57	-71.08
19196	37.3238	80.8207	1530.0	979763.56	-24.36	-76.49	3.61	-72.88
19197	37.3281	80.8200	1585.0	979762.12	-21.56	-75.56	2.28	-73.28
19198	37.3284	80.8136	1545.0	979763.75	-23.70	-76.34	3.10	-73.24
19199	37.3209	80.8162	1780.0	979753.31	-11.10	-71.74	3.23	-68.51
19200	37.3216	80.8089	1910.0	979744.94	-7.25	-72.32	3.72	-68.60

Station	Latitude	Longitude	Elevation	Gravity Value	Free Air Anomaly	Bouguer Anomaly	Terrain Corr.	Complete Bouguer Anomaly
19201	37.3158	80.7942	1895.0	979744.00	-9.60	-74.16	2.67	-71.49
19202	37.3214	80.7967	1790.0	979751.31	-12.16	-73.14	2.82	-70.32
19203	37.3299	80.7973	1890.0	979744.56	-10.44	-74.83	1.45	-73.38
19204	37.3303	80.8053	1625.0	979759.62	-20.30	-75.66	4.85	-70.81
19205	37.3340	80.7947	1600.0	979760.50	-21.78	-76.29	1.57	-74.72
19206	37.3301	80.7895	1870.0	979747.12	-9.76	-73.47	4.35	-69.12
19207	37.3312	80.7803	1925.0	979744.44	-7.27	-72.86	1.50	-71.36
19208	37.3347	80.7718	1910.0	979745.37	-7.75	-72.82	0.81	-72.01
19209	37.3382	80.7641	1660.0	979758.62	-18.95	-75.50	1.12	-74.38
19210	37.3376	80.7903	1560.0	979764.37	-22.60	-75.75	1.58	-74.17
30211	37.3418	80.7710	1595.0	979762.94	-20.75	-75.09	1.16	-73.93
30212	37.3420	80.7818	1570.0	979762.75	-23.29	-76.77	1.41	-75.36
30213	37.3354	80.7579	1610.0	979762.44	-18.90	-73.75	1.53	-72.22
30214	37.2558	80.8063	2215.0	979729.56	11.69	-63.78	1.13	-62.65
30215	37.2554	80.8142	2337.0	979722.12	15.72	-63.90	0.95	-62.95
30216	37.2553	80.8212	2468.0	979714.00	19.92	-64.16	0.99	-63.17
30217	37.2541	80.8279	2620.0	979703.87	24.09	-65.17	1.08	-64.09
30218	37.2533	80.8414	2991.0	979682.00	37.10	-64.80	0.87	-63.93
30219	37.2536	80.8477	3145.0	979671.87	41.46	-65.69	1.18	-64.51
30220	37.2558	80.8558	3380.0	979659.31	51.00	-64.15	4.43	-59.72
20001	37.2486	80.7097	1720.0	979754.12	-9.37	-67.96	2.97	-64.99
20002	37.2432	80.7103	1731.0	979752.62	-9.83	-68.81	2.66	-66.15
20003	37.2402	80.7087	1726.0	979751.87	-11.05	-69.85	2.91	-66.94
20004	37.2422	80.7161	1877.0	979745.19	-3.54	-67.49	0.15	-67.34
20005	37.2422	80.7267	1994.0	979739.06	1.34	-66.59	0.07	-66.52
20006	37.2401	80.7362	2150.0	979729.44	6.39	-66.86	0.12	-66.74
20007	37.2419	80.7445	2168.0	979728.94	7.58	-66.28	0.05	-66.23
20008	37.2478	80.7486	2076.0	979735.50	5.49	-65.24	0.16	-65.08
20009	37.2386	80.7471	1991.0	979739.62	2.56	-65.27	0.47	-64.80
20010	37.2282	80.7402	1789.0	979749.00	-7.06	-68.01	2.85	-65.16
20011	37.2178	80.7400	1808.0	979746.62	-6.78	-68.37	0.57	-67.80
20012	37.2085	80.7392	1797.0	979744.81	-8.69	-69.91	2.11	-67.80
20013	37.1971	80.7351	1832.0	979738.00	-11.27	-73.68	3.15	-70.53
20014	37.1946	80.7351	1841.0	979737.75	-9.74	-72.46	3.32	-69.14
20015	37.1783	80.7158	2167.0	979713.75	-2.14	-75.97	0.16	-75.81
20016	37.1681	80.7042	1936.0	979726.56	-10.11	-76.07	0.95	-75.12
20017	37.1641	80.7001	1983.0	979721.44	-10.82	-78.38	0.08	-78.30
20018	37.1618	80.6967	2041.0	979716.44	-9.43	-78.96	0.02	-78.94
20019	37.1587	80.6938	2050.0	979715.37	-9.64	-79.48	0.02	-79.46
20020	37.1437	80.6906	2087.0	979711.37	-9.23	-80.33	0.0	-80.33
20021	37.1388	80.6863	2041.0	979714.25	-9.74	-79.27	0.20	-79.07
20022	37.1383	80.6809	2091.0	979711.00	-8.29	-79.53	0.0	-79.53
20023	37.1317	80.6869	2105.0	979712.00	-5.97	-77.69	0.0	-77.69
20024	37.1278	80.6941	2116.0	979710.81	-5.19	-77.28	0.0	-77.28
20025	37.1941	80.7292	1847.0	979737.37	-9.55	-72.47	2.65	-69.82
20026	37.1499	80.7191	1953.0	979720.69	-12.52	-79.05	0.23	-78.82
20027	37.1460	80.7129	1946.0	979720.62	-13.24	-79.53	0.27	-79.26
20028	37.1368	80.7018	1993.0	979717.06	-11.44	-79.34	0.72	-78.62
20029	37.1338	80.6934	2100.0	979710.50	-7.94	-79.49	0.0	-79.49
20030	37.2289	80.7332	1860.0	979744.19	-5.20	-68.57	0.73	-67.84

Station	Latitude	Longitude	Elevation	Gravity Value	Free Air Anomaly	Bouguer Anomaly	Terrain Corr.	Complete Bouguer Anomaly
20031	37.2371	80.7208	1743.0	979751.81	-8.58	-67.96	2.31	-65.65
21032	37.2460	80.6280	2000.0	979732.50	-4.66	-72.80	2.05	-70.75
21033	37.2483	80.6329	1840.0	979742.94	-9.27	-71.96	4.08	-67.88
21034	37.2467	80.6358	1860.0	979740.06	-10.26	-73.63	3.61	-70.02
21035	37.2446	80.6407	1900.0	979736.69	-9.88	-74.61	3.67	-70.94
21036	37.2422	80.6503	2016.0	979733.56	-2.09	-70.77	3.64	-67.13
21037	37.2412	80.6585	2127.0	979725.31	0.10	-72.37	0.58	-71.79
21038	37.2408	80.6633	2000.0	979733.12	-4.03	-72.17	1.52	-70.65
21039	37.2406	80.6654	1980.0	979734.81	-4.23	-71.68	1.69	-69.99
21040	37.2441	80.6737	1888.0	979741.19	-6.50	-70.83	4.28	-66.55
21041	37.2442	80.6770	1872.0	979742.31	-6.88	-70.66	3.96	-66.70
21042	37.2377	80.6786	1931.0	979737.81	-4.90	-70.68	3.93	-66.75
21043	37.2355	80.6808	1980.0	979735.06	-3.04	-70.50	4.23	-66.27
21044	37.2366	80.6838	1982.0	979734.25	-3.66	-71.19	3.34	-67.85
21045	37.2360	80.6866	1955.0	979736.31	-4.14	-70.75	3.38	-67.37
21046	37.2306	80.7059	1769.0	979747.62	-10.32	-70.59	3.47	-67.12
21047	37.2238	80.6966	2000.0	979733.50	-1.85	-69.98	3.58	-66.40
21048	37.2181	80.7072	2040.0	979731.06	-0.52	-70.02	3.49	-66.53
21049	37.2160	80.7119	1940.0	979735.56	-4.49	-70.58	3.43	-67.15
21050	37.2140	80.7194	2000.0	979733.37	-1.03	-69.17	3.39	-65.78
21051	37.2192	80.7184	1900.0	979738.56	-6.19	-70.92	2.88	-68.04
21052	37.2484	80.6839	1827.0	979745.56	-7.87	-70.11	3.86	-66.25
21053	37.2412	80.6979	1800.0	979745.87	-10.09	-71.42	3.21	-68.21
21054	37.1632	80.6813	2027.0	979717.12	-10.06	-79.11	0.04	-79.07
21055	37.1703	80.6702	2002.0	979719.56	-10.91	-79.11	0.02	-79.09
21056	37.1701	80.6646	1994.0	979719.56	-11.66	-79.59	0.06	-79.53
21057	37.1728	80.6602	1956.0	979721.56	-13.23	-79.87	0.02	-79.85
21058	37.1710	80.6556	1937.0	979722.75	-13.83	-79.82	0.02	-79.80
21059	37.1684	80.6524	1939.0	979721.75	-14.64	-80.70	0.02	-80.68
21060	37.1648	80.6459	1832.0	979727.44	-19.02	-81.43	2.02	-79.41
21061	37.1718	80.6379	1781.0	979731.12	-20.13	-80.81	1.43	-79.38
21062	37.1772	80.6294	1767.0	979732.06	-21.45	-81.65	1.72	-79.93
21063	37.1638	80.6310	2018.0	979716.62	-12.34	-81.09	0.01	-81.08
21064	37.1526	80.6465	1942.0	979721.25	-12.99	-79.15	0.12	-79.03
21065	37.1458	80.6581	2027.0	979717.50	-8.74	-77.80	0.09	-77.71
21066	37.1380	80.6572	2013.0	979716.25	-10.37	-78.95	0.02	-78.93
21067	37.1331	80.6606	2047.0	979713.00	-10.42	-80.16	0.0	-80.16
21069	37.1303	80.6347	1899.0	979719.06	-17.34	-82.04	0.14	-81.90
21070	37.1587	80.6401	1856.0	979726.37	-16.89	-80.12	3.52	-76.60
22071	37.1332	80.7424	1976.0	979717.75	-12.35	-79.67	0.74	-78.93
22072	37.1350	80.7435	1978.0	979718.25	-11.66	-79.05	1.00	-78.05
22073	37.1379	80.7449	1980.0	979717.87	-11.85	-79.31	0.17	-79.14
22074	37.1423	80.7521	2060.0	979714.56	-8.58	-78.76	0.06	-78.70
22075	37.1307	80.7468	2027.0	979715.37	-8.99	-78.05	0.42	-77.63
22076	37.1352	80.7593	2012.0	979716.94	-9.78	-78.33	0.09	-78.24
22077	37.1323	80.7666	2007.0	979717.25	-9.94	-78.31	0.24	-78.07
22078	37.1278	80.7744	2024.0	979715.87	-8.78	-77.73	0.79	-76.94
22079	37.1279	80.7920	2120.0	979710.37	-5.25	-77.47	0.11	-77.36
22080	37.1315	80.7959	2160.0	979712.62	-0.17	-73.76	0.24	-73.52
22081	37.1398	80.7980	2460.0	979696.19	11.60	-72.21	0.16	-72.05

Station	Latitude	Longitude	Elevation	Gravity Value	Free Air Anomaly	Bouguer Anomaly	Terrain Corr.	Complete Bouguer Anomaly
22082	37.1429	80.8005	2835.0	979671.94	21.68	-74.90	0.22	-74.68
22083	37.1441	80.8075	2560.0	979691.87	15.76	-71.46	1.95	-69.51
22084	37.1506	80.8055	2180.0	979715.81	3.96	-70.31	1.12	-69.19
22085	37.1567	80.8061	1960.0	979730.62	-2.86	-69.63	1.17	-68.46
22086	37.1594	80.8050	1920.0	979731.56	-5.68	-71.09	1.29	-69.80
22087	37.1594	80.8089	2000.0	979727.19	-2.53	-70.67	1.09	-69.58
22088	37.1549	80.8143	1940.0	979730.44	-4.93	-71.02	1.36	-69.66
22089	37.1518	80.8184	1989.0	979728.25	-1.57	-69.33	1.31	-68.02
22090	37.1486	80.8240	1958.0	979729.00	-3.73	-70.44	2.01	-68.43
22091	37.1472	80.8318	1971.0	979728.44	-3.07	-70.22	1.50	-68.72
22092	37.1430	80.8387	1980.0	979726.94	-3.73	-71.18	1.47	-69.71
22093	37.1403	80.8469	2012.0	979725.44	-1.28	-69.83	1.27	-68.56
22094	37.1376	80.8506	1980.0	979726.37	-3.35	-70.81	1.47	-69.34
22095	37.1321	80.8546	2000.0	979725.56	-2.28	-70.42	2.22	-68.20
22096	37.1281	80.8612	2000.0	979725.25	-1.66	-69.80	2.04	-67.76
22097	37.1310	80.7763	2080.0	979713.87	-5.51	-76.37	0.08	-76.29
22098	37.1338	80.7778	2120.0	979713.06	-3.50	-75.72	0.09	-75.63
22099	37.1358	80.7791	2153.0	979711.12	-2.33	-75.68	0.10	-75.58
22100	37.1632	80.7934	1908.0	979733.62	-4.75	-69.75	1.31	-68.44
22101	37.1637	80.7848	1920.0	979732.37	-5.81	-71.22	2.49	-68.73
22102	37.1665	80.7801	1900.0	979733.44	-6.62	-71.36	3.30	-68.06
22103	37.1693	80.7766	1900.0	979733.87	-6.19	-70.92	3.25	-67.67
22104	37.1708	80.7708	1920.0	979732.87	-5.31	-70.72	2.97	-67.75
22105	37.1740	80.7696	1880.0	979734.06	-7.88	-71.93	2.44	-69.49
22106	37.1776	80.7619	1900.0	979734.31	-6.69	-71.42	3.56	-67.86
22107	37.1792	80.7584	1900.0	979734.50	-6.50	-71.23	3.53	-67.70
22108	37.1838	80.7524	1900.0	979734.56	-6.44	-71.17	2.40	-68.77
22109	37.1851	80.7496	1926.0	979733.37	-5.18	-70.80	3.01	-67.79
22110	37.1865	80.7480	1880.0	979735.31	-8.51	-72.56	3.68	-68.88
22111	37.1899	80.7456	1900.0	979732.94	-9.00	-73.73	1.28	-72.45
22112	37.1920	80.7410	1900.0	979733.75	-8.19	-72.92	0.88	-72.04
22113	37.1923	80.7371	1840.0	979737.19	-10.39	-73.08	2.50	-70.58
23114	37.2131	80.7636	1983.0	979737.06	1.06	-66.50	0.32	-66.18
23115	37.2190	80.7687	2200.0	979724.37	7.84	-67.11	0.27	-66.84
23116	37.2204	80.7688	2275.0	979718.87	9.39	-68.12	0.24	-67.88
23117	37.2192	80.7727	2320.0	979714.31	9.06	-69.98	0.52	-69.46
23118	37.2187	80.7772	2380.0	979711.37	11.77	-69.32	0.42	-68.90
23119	37.2114	80.7720	1851.0	979743.25	-5.17	-68.23	2.15	-66.08
23120	37.2084	80.7695	1820.0	979745.75	-5.59	-67.59	1.32	-66.27
23121	37.2127	80.7762	1940.0	979742.94	2.89	-63.21	1.74	-61.47
23122	37.2123	80.7814	1940.0	979742.44	2.39	-63.71	1.64	-62.07
23123	37.2096	80.7842	1960.0	979742.81	4.64	-62.13	0.96	-61.17
23124	37.2086	80.7914	1916.0	979739.75	-2.56	-67.83	1.38	-66.45
23125	37.2078	80.7975	1900.0	979740.69	-3.12	-67.86	1.58	-66.28
23126	37.2077	80.8010	1901.0	979740.31	-3.41	-68.17	1.80	-66.37
23127	37.2055	80.8074	1980.0	979736.06	0.71	-66.75	1.22	-65.53
23128	37.2050	80.8142	2020.0	979732.37	0.79	-68.03	1.20	-66.83
23129	37.2040	80.8170	2020.0	979731.94	0.35	-68.47	1.16	-67.31
23130	37.2012	80.8222	1971.0	979735.62	-0.57	-67.72	1.55	-66.17
23131	37.1981	80.8231	1920.0	979739.25	-1.74	-67.16	1.80	-65.36

Station	Latitude	Longitude	Elevation	Gravity Value	Free Air Anomaly	Bouguer Anomaly	Terrain Corr.	Complete Bouguer Anomaly
23132	37.1955	80.8193	1900.0	979739.69	-2.25	-66.98	1.32	-65.66
23133	37.1956	80.8142	1920.0	979739.94	-0.12	-65.53	1.51	-64.02
23134	37.2003	80.8238	1960.0	979735.81	-1.42	-68.20	2.90	-65.30
23135	37.1983	80.8272	1920.0	979737.25	-3.74	-69.16	2.22	-66.94
23136	37.1976	80.8305	1921.0	979736.94	-3.96	-69.41	2.15	-67.26
23137	37.1982	80.8358	1920.0	979736.75	-4.24	-69.66	2.10	-67.56
23138	37.1945	80.8383	1920.0	979736.37	-3.68	-69.09	1.09	-68.00
23139	37.1923	80.8381	1926.0	979736.56	-2.93	-68.55	0.97	-67.58
23140	37.1892	80.8349	1920.0	979737.50	-2.56	-67.97	1.87	-66.10
23141	37.1881	80.8298	2000.0	979734.19	1.65	-66.48	1.66	-64.82
23142	37.1884	80.8247	2080.0	979730.06	5.05	-65.81	0.88	-64.93
23143	37.1872	80.8327	1920.0	979738.75	-1.31	-66.72	3.29	-63.43
23144	37.1851	80.8255	1940.0	979738.31	1.07	-65.02	1.88	-63.14
23145	37.1800	80.8260	2020.0	979733.12	3.41	-65.41	1.65	-63.76
23146	37.1781	80.8324	2040.0	979731.75	3.92	-65.58	4.14	-61.44
23147	37.1756	80.8373	2040.0	979732.00	4.17	-65.33	2.30	-63.03
23148	37.1698	80.8388	1960.0	979733.37	-1.04	-67.82	2.88	-64.94
23149	37.1692	80.8454	1960.0	979734.81	0.39	-66.38	2.67	-63.71
23150	37.1672	80.8480	2120.0	979725.00	5.63	-66.60	1.19	-65.41
23151	37.1640	80.8514	2100.0	979726.06	4.81	-66.74	1.43	-65.31
23152	37.1607	80.8544	1980.0	979732.56	0.96	-66.50	2.58	-63.92
23153	37.1601	80.8595	1980.0	979732.75	1.15	-66.31	4.88	-61.43
23154	37.1620	80.8609	1980.0	979733.69	2.09	-65.37	2.39	-62.98
23155	37.1603	80.8680	1980.0	979733.56	1.96	-65.50	0.97	-64.53
23156	37.1579	80.8667	2000.0	979731.06	1.34	-66.80	1.31	-65.49
23157	37.1538	80.8695	1980.0	979731.31	-0.29	-67.75	3.38	-64.37
23158	37.1518	80.8719	2020.0	979728.75	1.85	-66.97	3.26	-63.71
23159	37.1647	80.8598	2080.0	979725.81	2.68	-68.19	0.60	-67.59
23160	37.1703	80.8599	2080.0	979726.81	3.68	-67.19	0.54	-66.65
23161	37.1734	80.8633	2300.0	979716.25	13.81	-64.55	0.16	-64.39
23162	37.1721	80.8658	2280.0	979717.50	13.18	-64.50	0.18	-64.32
23163	37.1672	80.8703	2220.0	979720.87	10.91	-64.73	0.21	-64.52
23164	37.1620	80.8718	2000.0	979733.25	3.53	-64.61	1.38	-63.23
23165	37.1762	80.8567	2160.0	979724.69	8.14	-65.45	0.37	-65.08
23166	37.1806	80.8488	2140.0	979726.19	7.76	-65.15	0.33	-64.82
23167	37.1786	80.8468	2220.0	979720.87	9.97	-65.66	0.38	-65.28
23168	37.1749	80.8449	2120.0	979727.75	7.44	-64.79	0.59	-64.20
23169	37.1731	80.8462	2040.0	979731.87	4.98	-64.52	2.19	-62.33
23170	37.1827	80.8451	2040.0	979731.69	3.85	-65.65	0.50	-65.15
23171	37.1843	80.8374	2000.0	979734.94	3.34	-64.80	1.27	-63.53
23172	37.1887	80.8464	2000.0	979733.00	0.47	-67.67	0.65	-67.02
23173	37.1866	80.8519	2040.0	979730.81	2.04	-67.46	0.58	-66.88
23174	37.1844	80.8572	2100.0	979728.00	5.81	-65.74	1.07	-64.67
23175	37.1796	80.8701	2172.0	979723.62	8.21	-65.79	0.46	-65.33

The vita has been removed from the scanned document